

https://dspace.org/

Fatigue crack closure and closure development in a high strength aluminium alloy

Garz, Reiner Ernst

2015-01-27
http://hdl.handle.net/10539/16793

Downloaded from a DSpace repository. https://dspace.org/

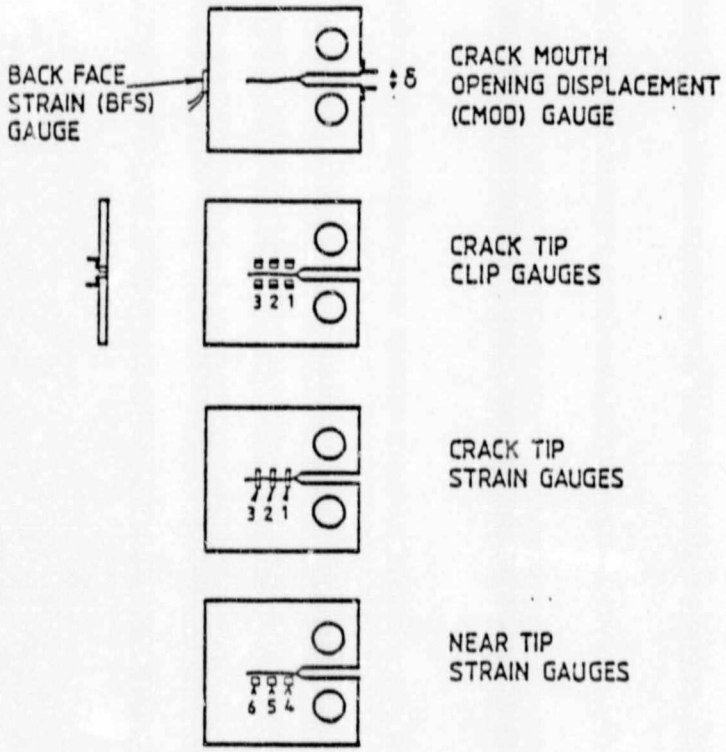

Figure 2.9 Positioning of compliance gauges used for closure measurements.

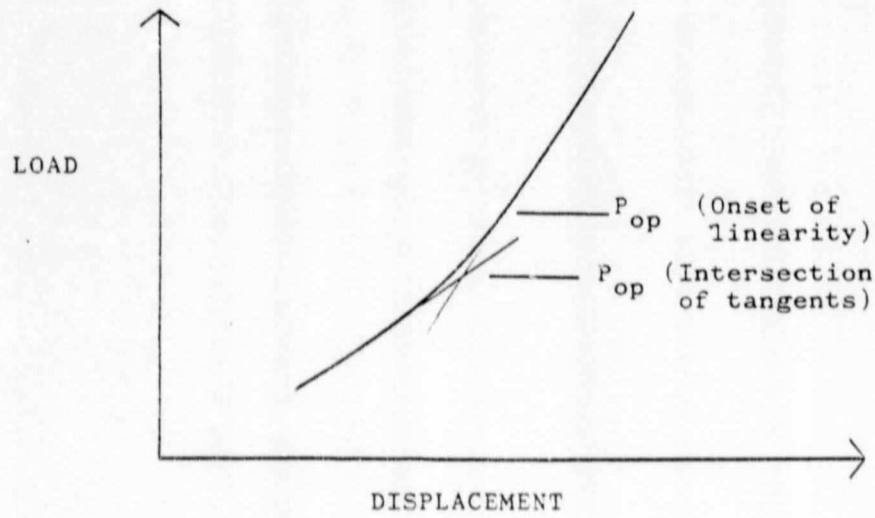

Figure 2.10 Sketch showing how the point P_{op} is determined using the onset of linearity and using the intersection of tangents.

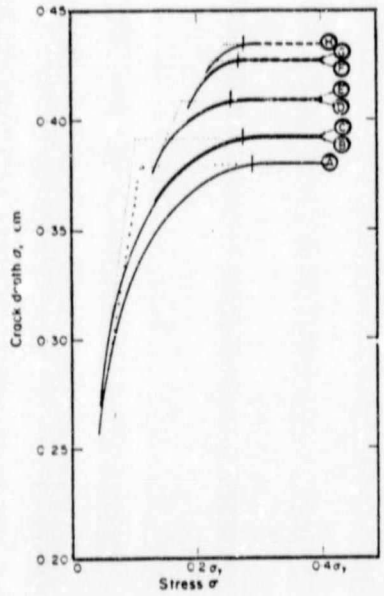

Figure 2.11 An example showing how the method used to determine closure alters the closure trend as R ratio varies. If closure is measured using the intersection of tangents (dotted lines) K_{op} increases with R, whereas if K_{op} is measured using the onset of linearity (indicate by markers) K_{op} remains remains fairly constant as R increases (data from ref. [55]).

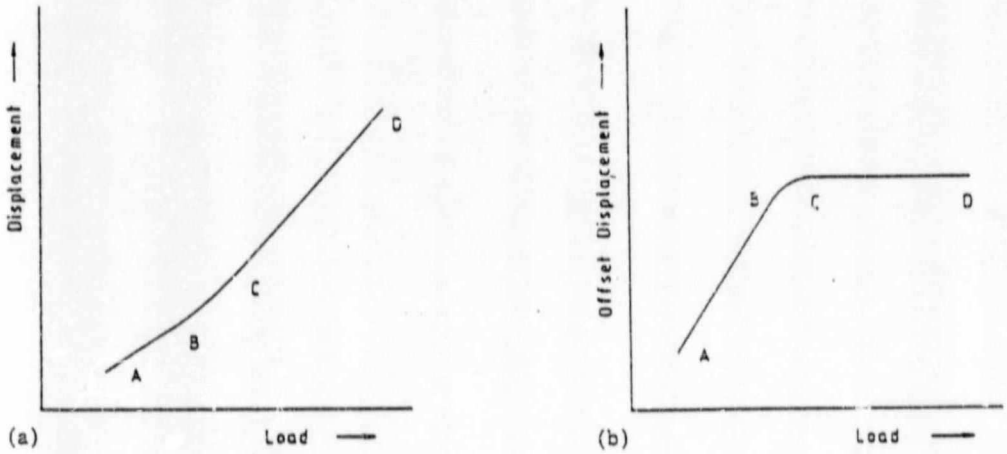

Figure 2.12 Comparison of the offset elastic displacement technique to measure closure compared with the conventional compliance determination of the crack opening point (after ref. [19]).

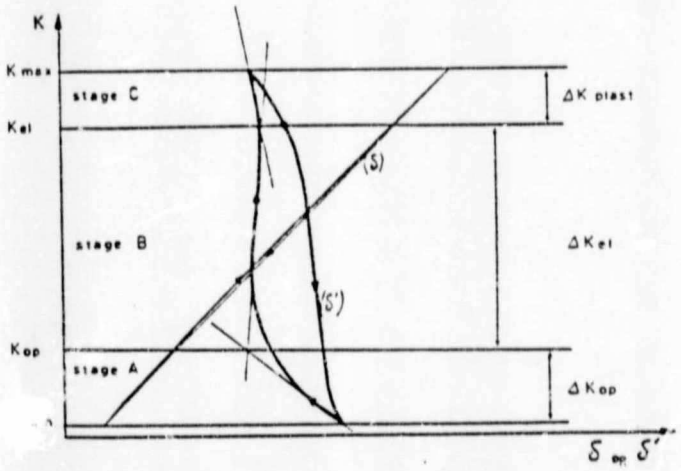

Figure 2.13 Characteristic regions of the offset displacement curve (after ref. [56]).

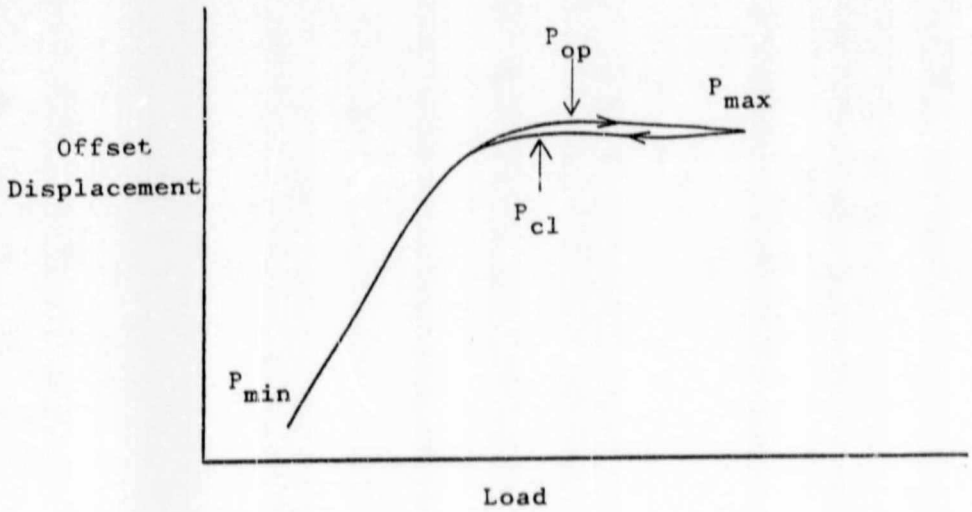

Figure 2.14 Illustration of typical differences between P_{op} and P_{cl}.

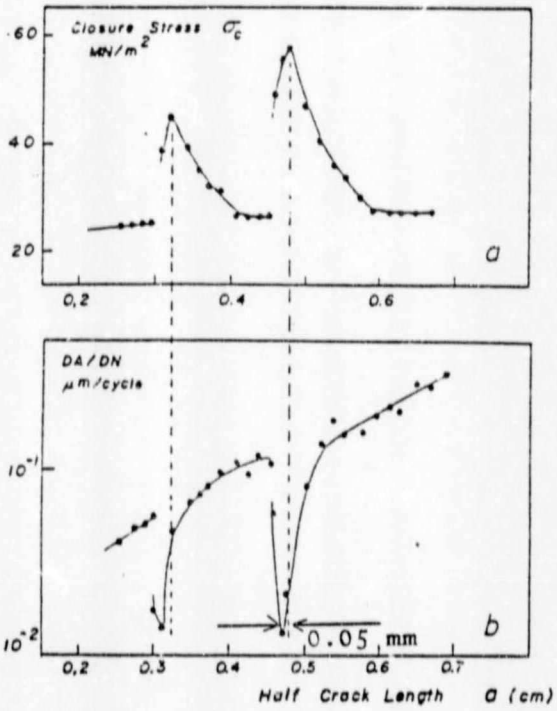

Figure 2.15 An Estimation of the resolution of the closure measuring technique by using the crack increment between the minimum growth rate value and the maximum closure value, from data according to [62].

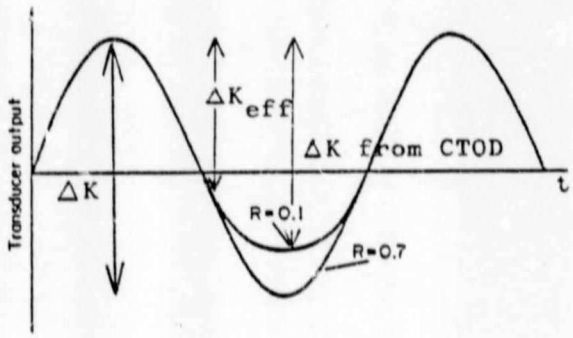

Figure 2.16 Fatigue load cycle showing the magnitude, of the parameter CTOD relative to ΔK and ΔK_{eff}.

a)

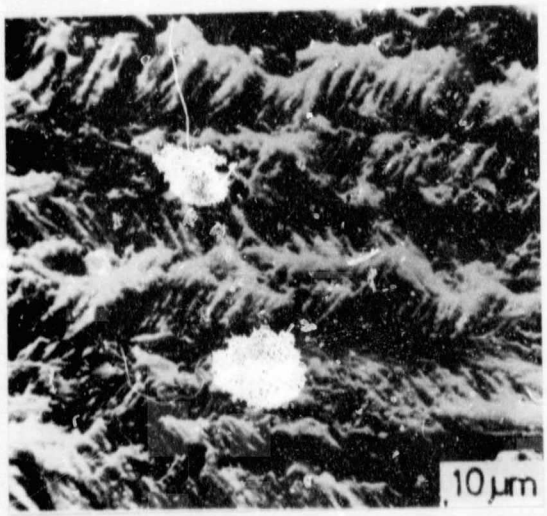

b)

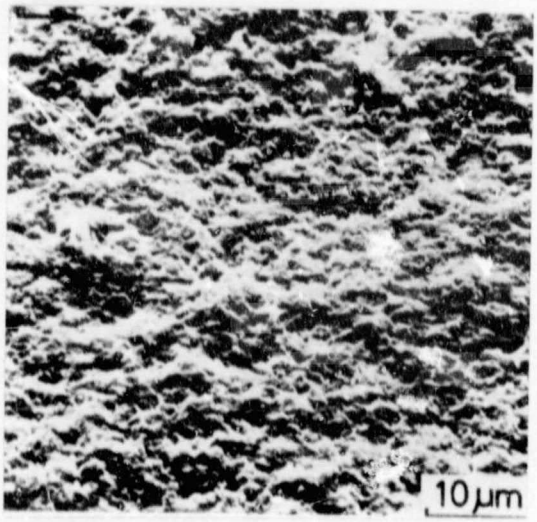

Figure 2.17 Fatigue fracture surfaces illustrating the type of surface roughness which produced closure a) compared to that which did not produce closure b), (after ref. [25]).

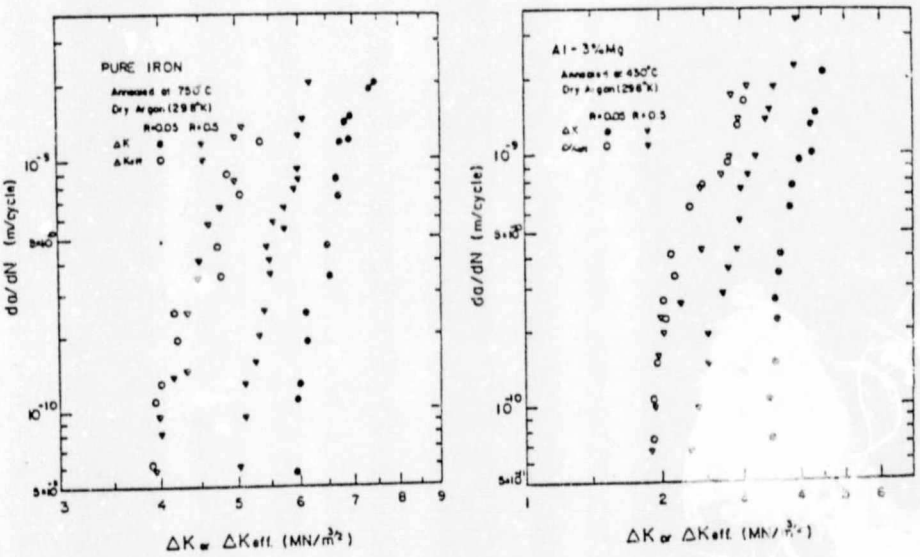

Figure 2.18 Growth rate data which is rationalised using the closure parameter ΔK_{eff}, (after ref. [79]).

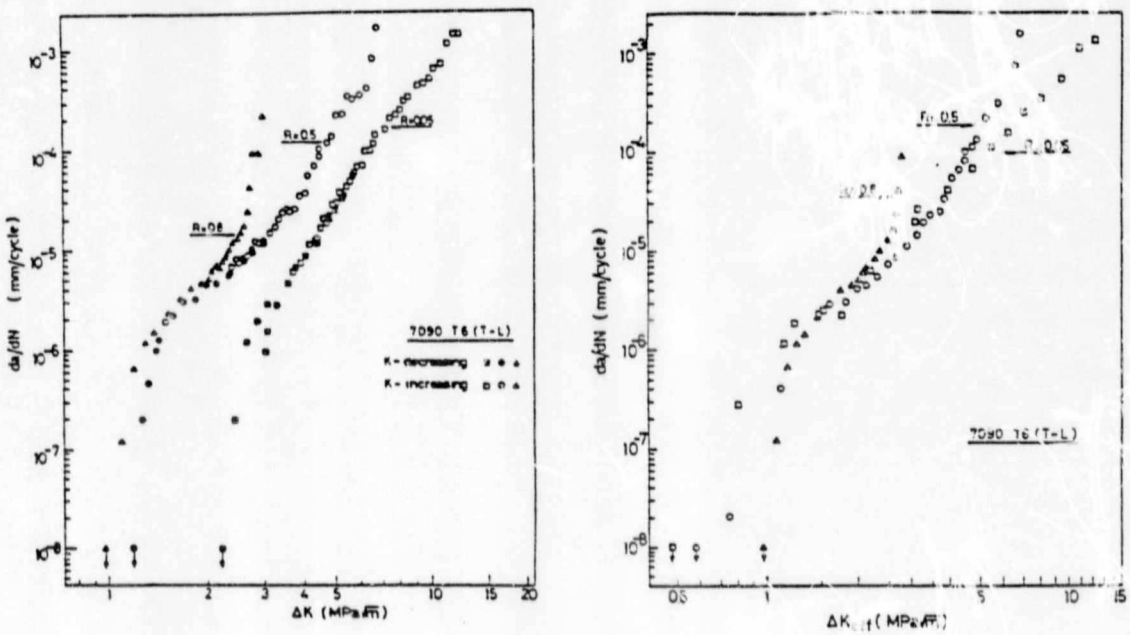

Figure 2.19 Growth rate data which is not totally rationalised by ΔK_{eff}, (after ref. [70]).

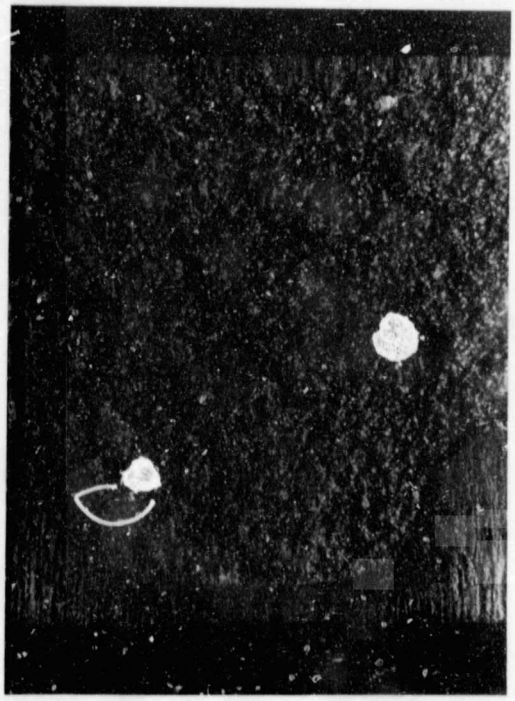

Figure 2.20 Strongly bowed fatigue crack front for 25 mm thick CT specimen following growth under compressive loading (after ref [100]).

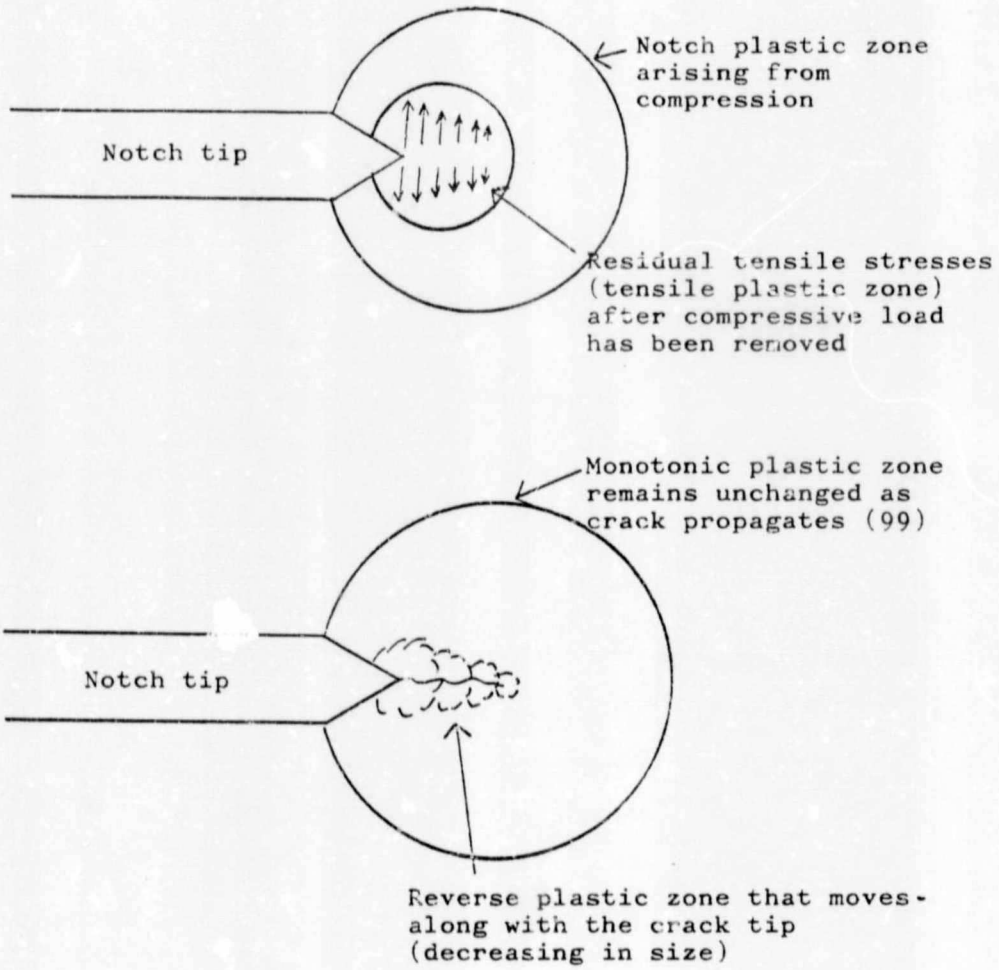

Figure 2.21 a) The development of tensile stresses under compressive loading. b) Movement of the tensile stresses (reverse plastic zone) during compressive loading.

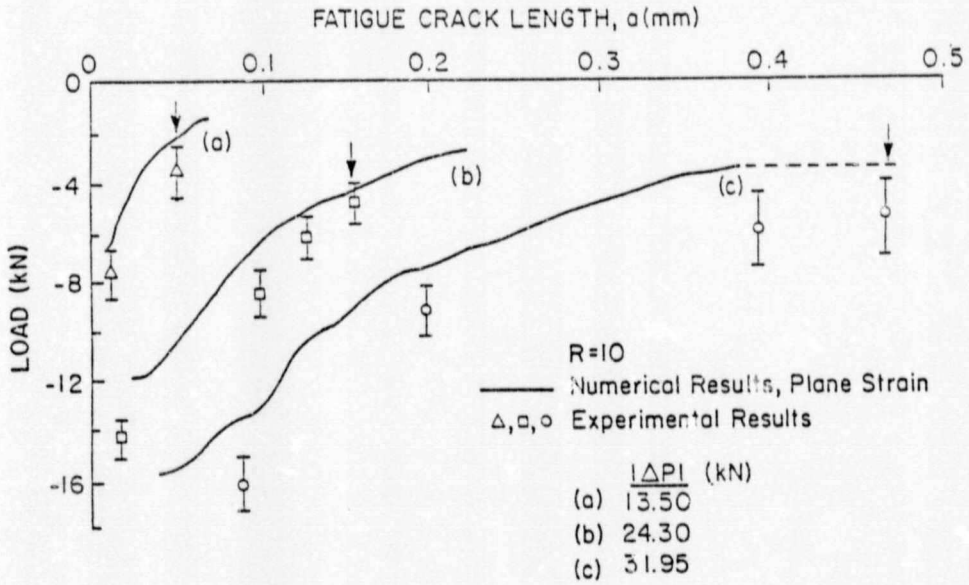

Figure 2.22 A comparison between numerically and experimentally determined crack tip opening loads obtained under compressive loading (after ref. [28]).

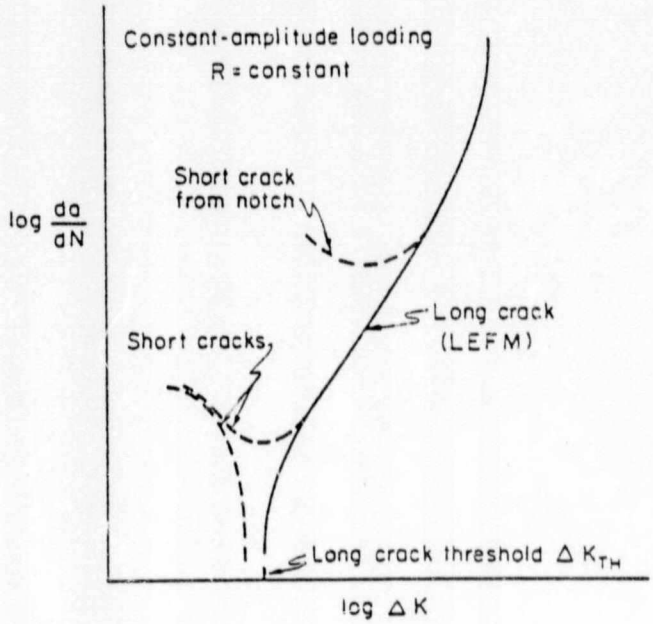

Figure 2.23 Schematic representation of da/dN vs ΔK for short and long cracks (after ref. [80]).

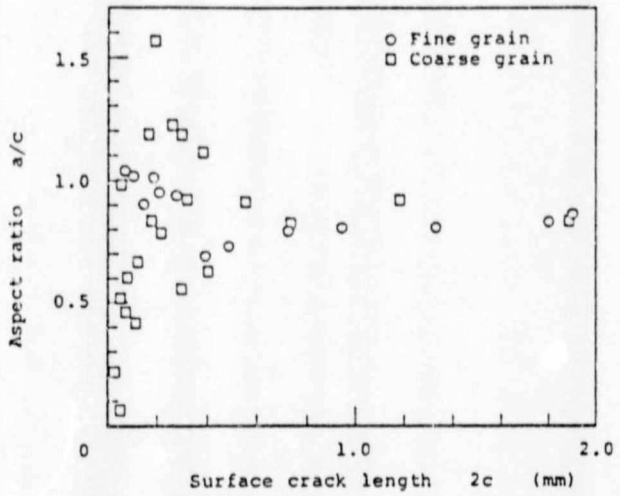

igure 2.24 Variation of aspect ratio with surface crack length ..fter ref.[71].

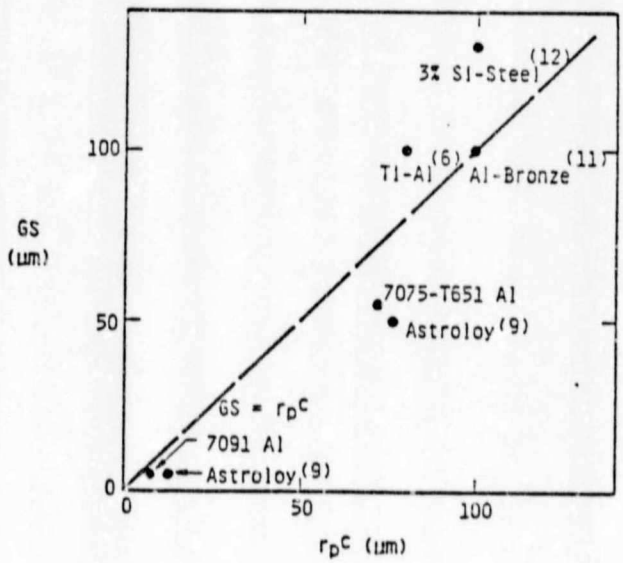

Figure 2.25 Grain size (GS) vs plastic zone size (r_p^c) which can be used to determine the crack length at which the da/dn vs ΔK curves converge for small and large cracks for several alloy systems (after ref. [118]).

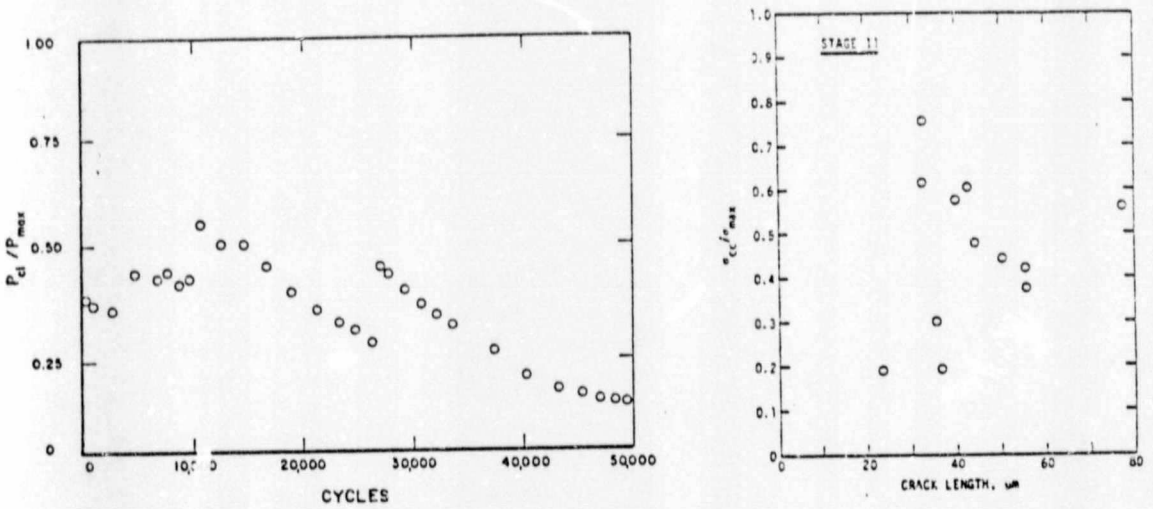

Figure 2.26 Short crack closure data obtained by a) Morris [123] and b) Larson [131].

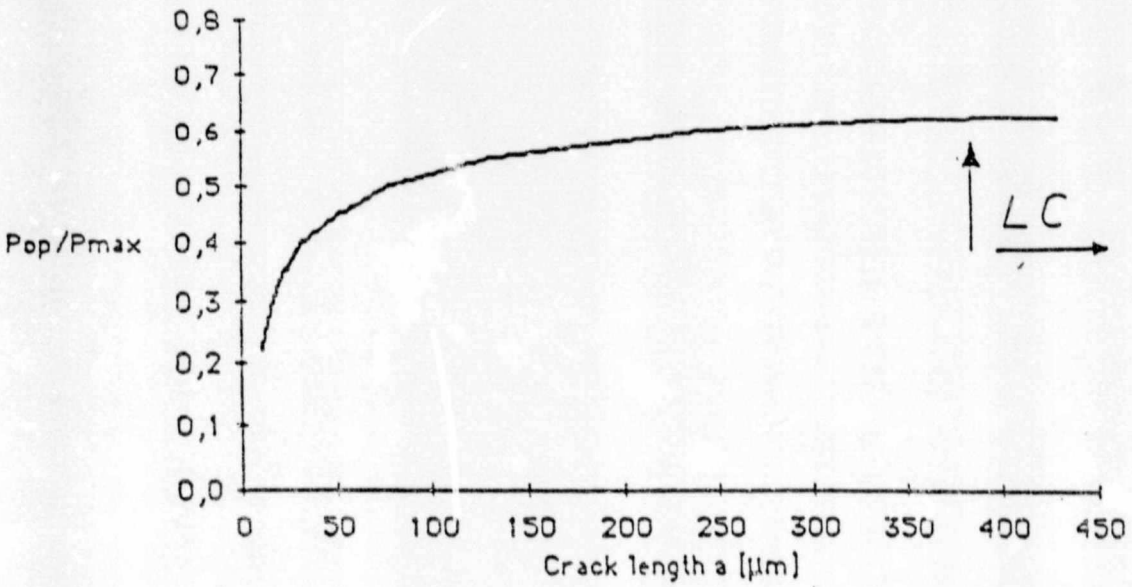

Figure 2.27 Development of crack closure (P_{op}/P_{max}) with increasing crack length, from FEM calculations (after ref. [79]).

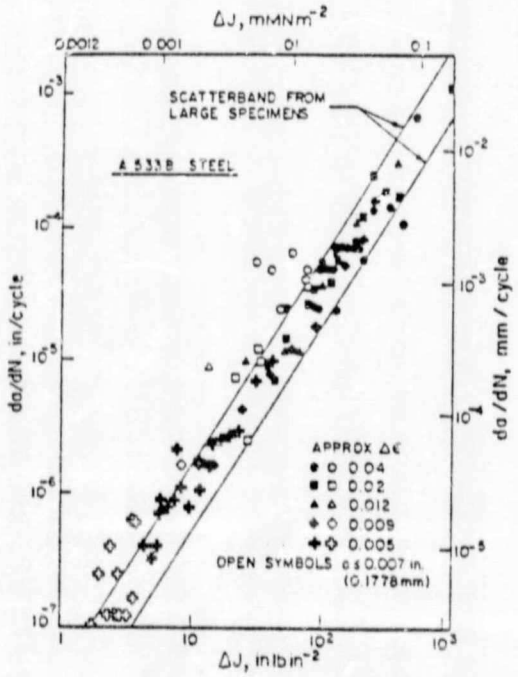

Figure 2.28 Growth rate data correlating short (a ≤ 0.18 mm) and long (a ≥ 25 mm) crack growth in A533B steel, using the elastic plastic fracture mechanics parameter ΔJ (after Dowling [135]).

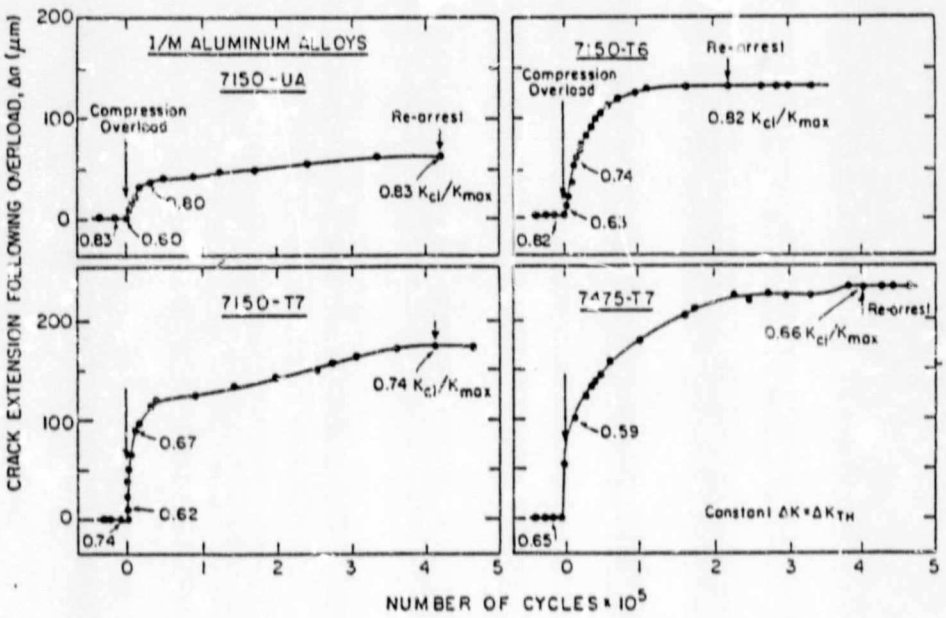

Figure 2.29 Graphs showing the increase in crack length and closure ratio K_{cl}/K_{max} with number of cycles following a reduction in closure caused by the application of compressive overloads (after ref. [28]).

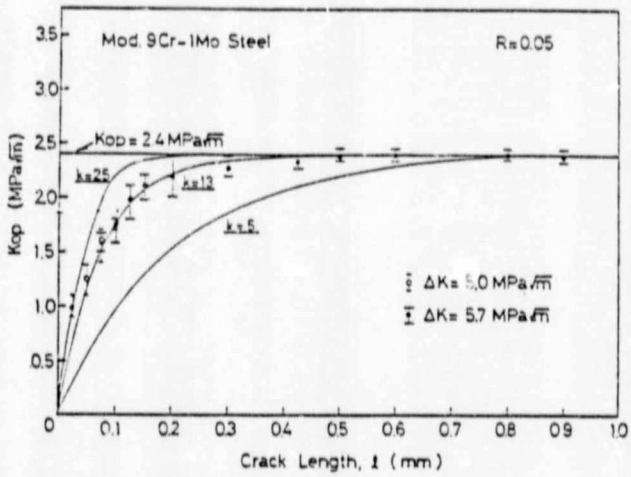

Figure 2.30 Variation of K_{op} level with crack length as a function of ΔK (after ref. [53]).

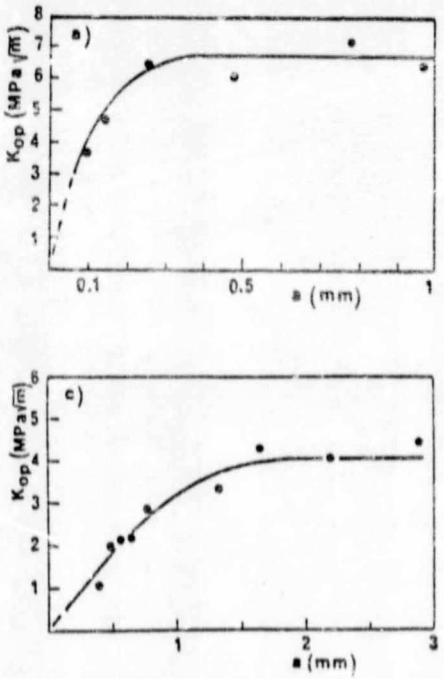

Figure 2.31 Variation of K_{op} with crack length a) for a 2024 T351 Al alloy (ref. [140]) and b) for a nodular cast iron (ref. [141]).

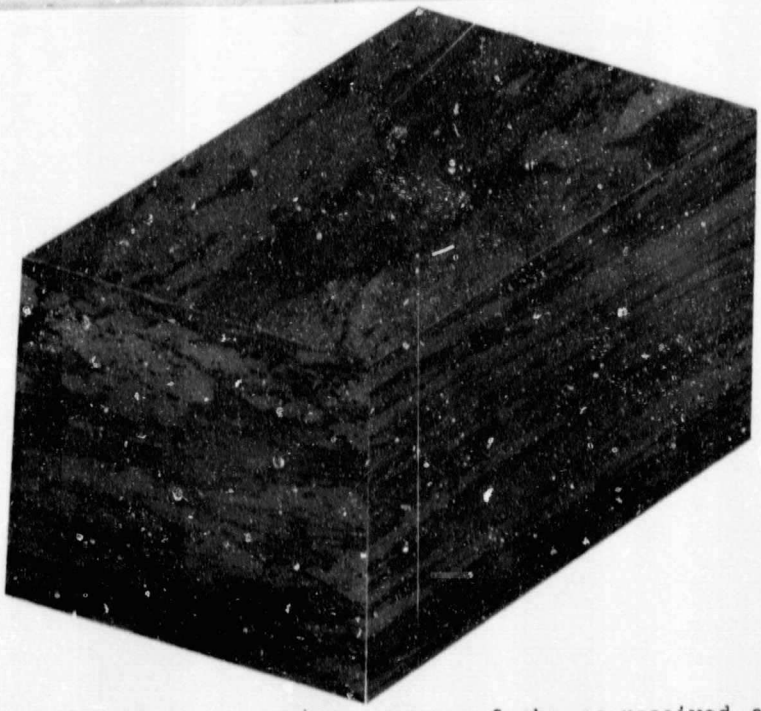

Figure 3.1 Composite 3-D microstructure of the as-received and heat treated material conditions.

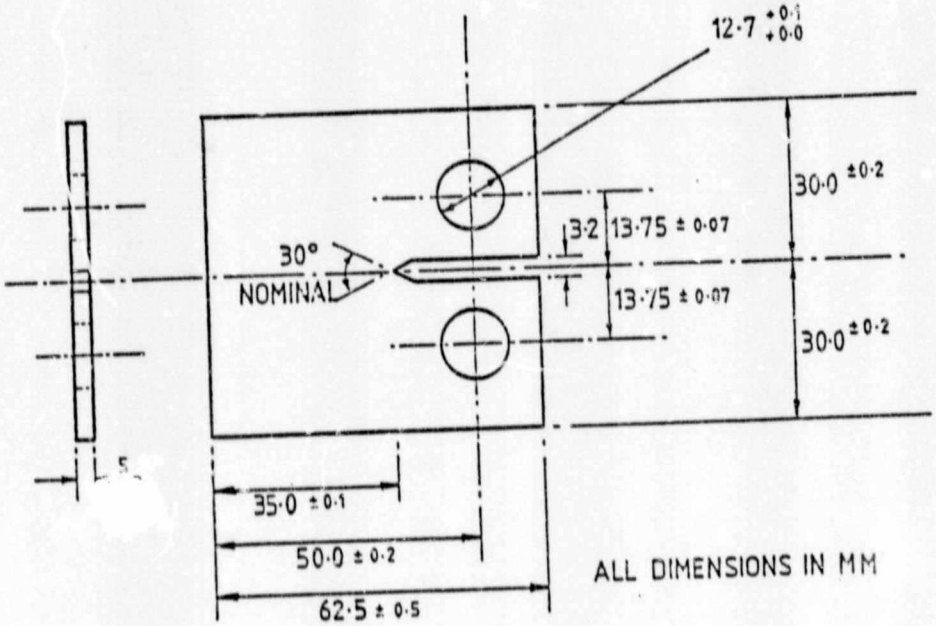

Figure 3.2 Dimensions of compact tension (CT) specimen.

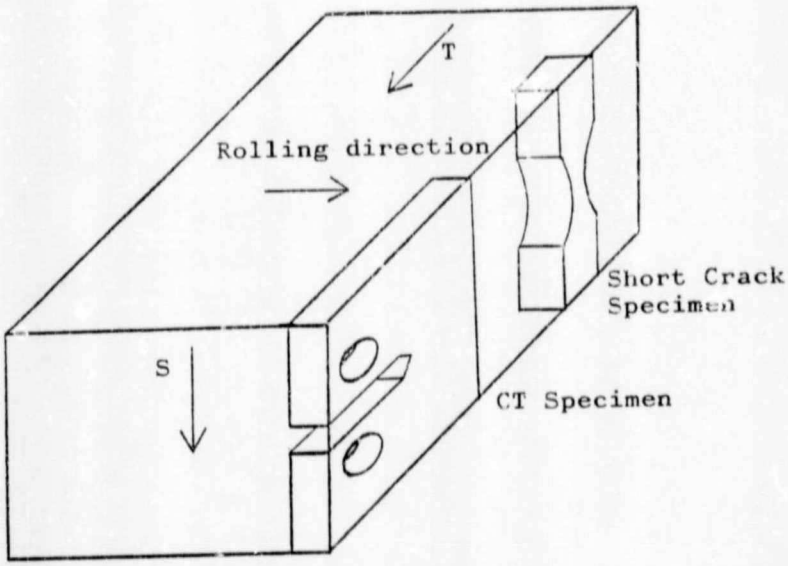

Figure 3.3 Orientation of CT and short crack specimens relative to the rolling direction of the aluminium plate.

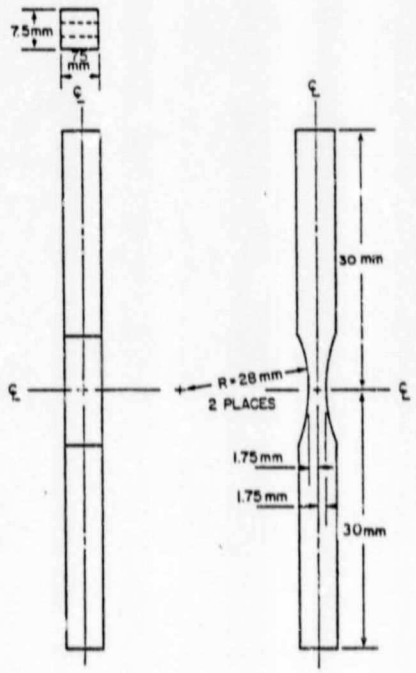

Figure 3.4 Short crack specimen geometry, similar to that used by Larson [131].

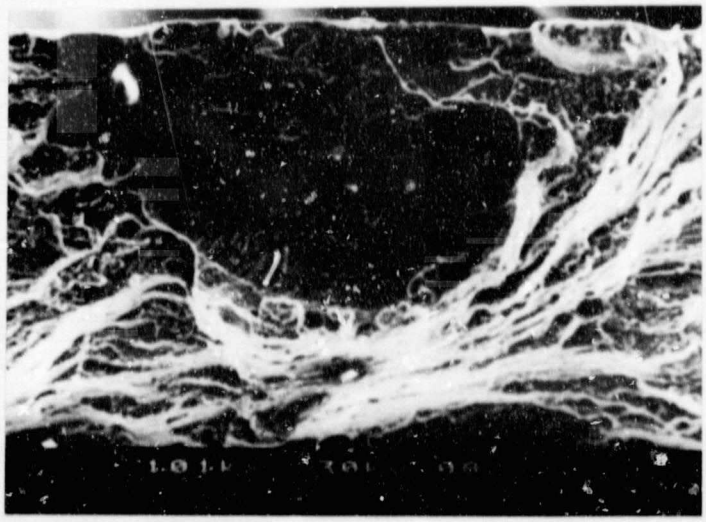

Figure 3.5 Typical fractograph of a short crack used to determine a/c ratios.

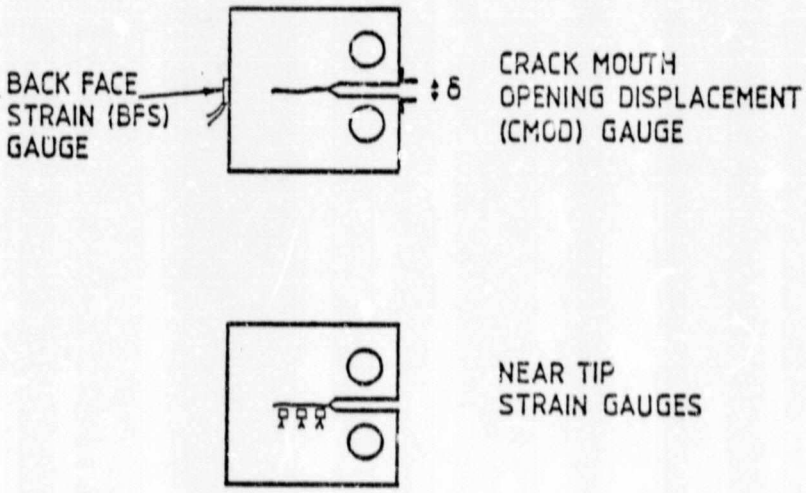

Figure 3.6 Positioning of the various gauges used to measure closure on CT specimens.

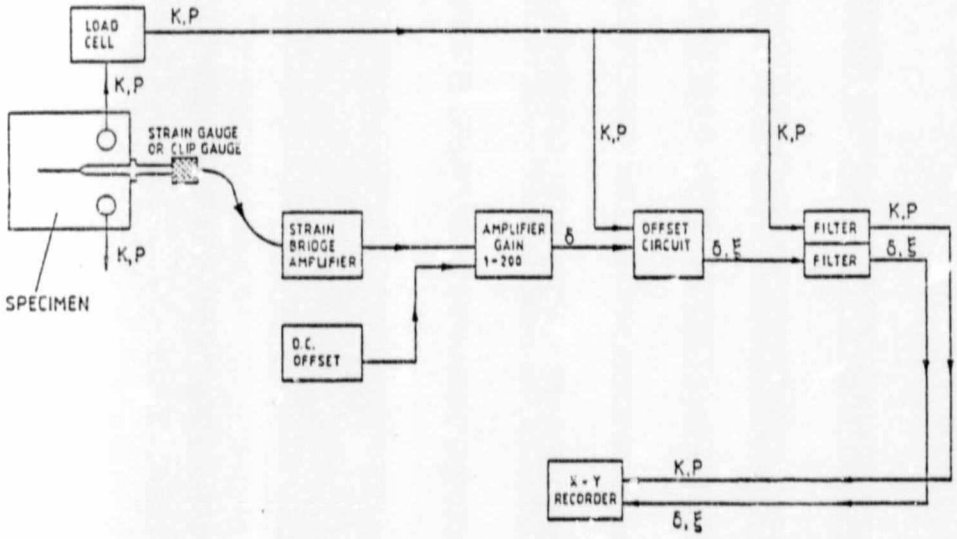

Figure 3.7 Layout of crack closure system. (K represents stress intensity, δ represents strain or displacement and ζ represents offset displacement.)

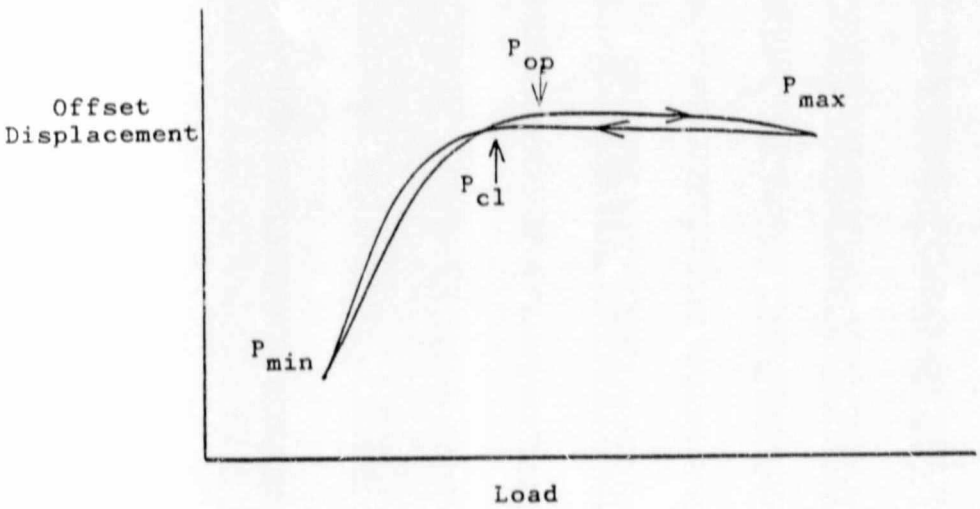

Figure 3.8 Load vs offset displacement trace indicating the points at which P_{op} and P_{cl} were chosen.

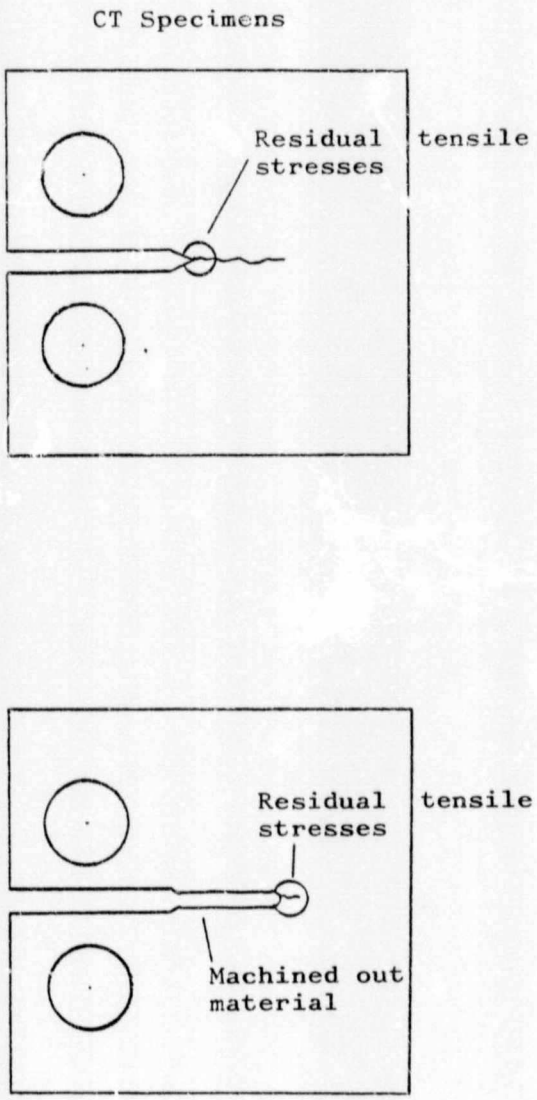

Figure 3.9 Residual stress distribution around fatigue crack notch after compressive loading.

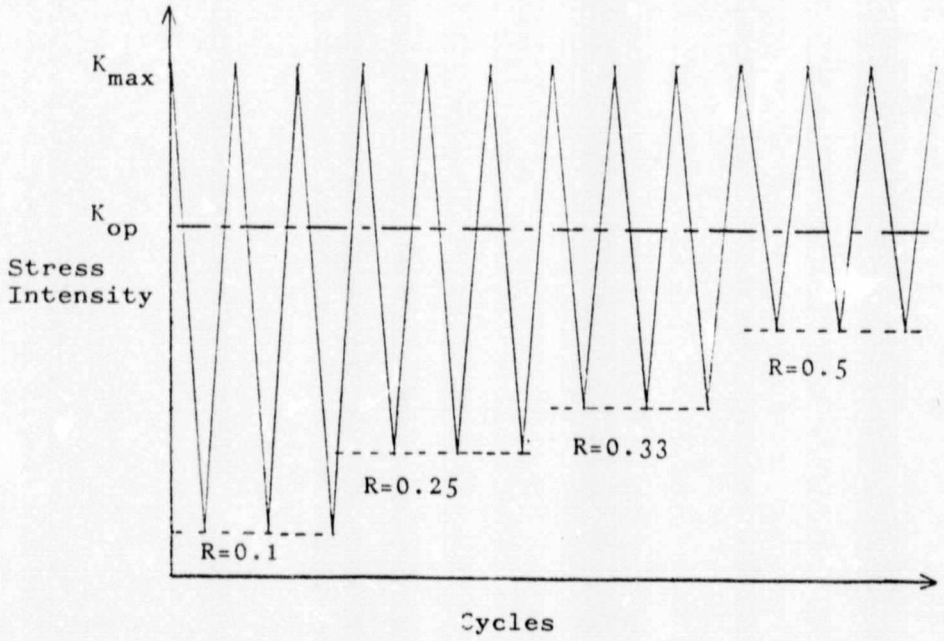

Figure 4.1 Representation of R ratio variation relative to K_{op}.

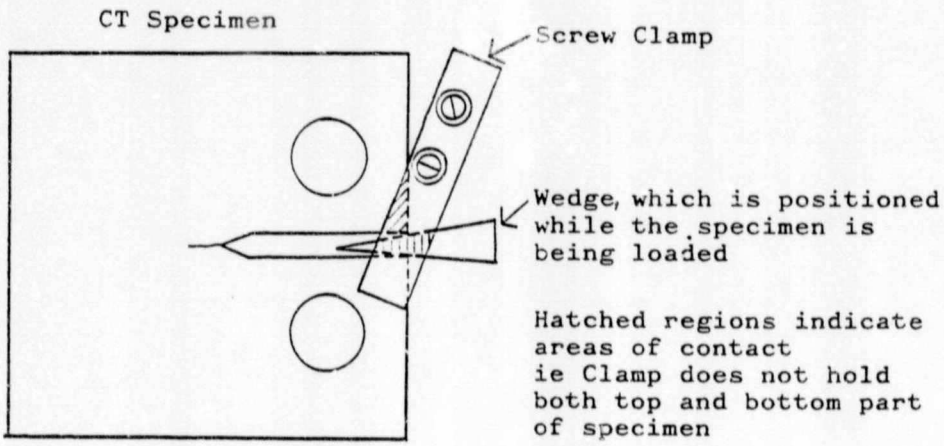

Figure 4.2 Sketch of triangular shaped wedge clamped into the mouth of a CT specimen, used to compare physical wedgeing with closure.

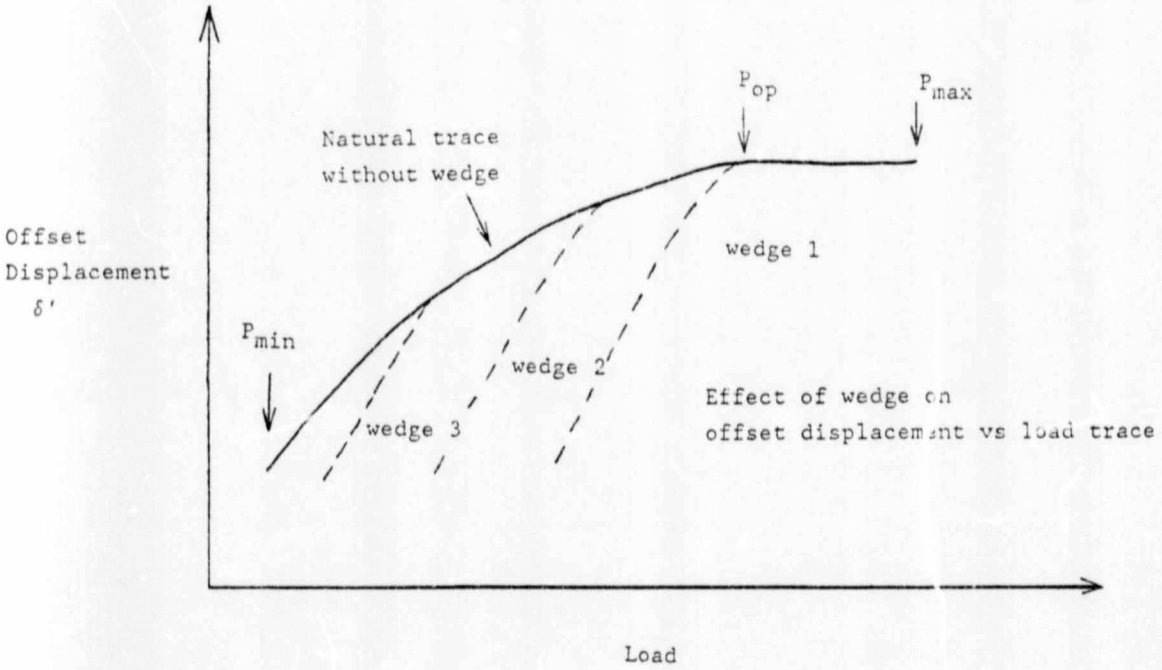

Figure 4.3 Offset displacement vs load traces illustrating the effect of wedge contact on the curvature of the trace.

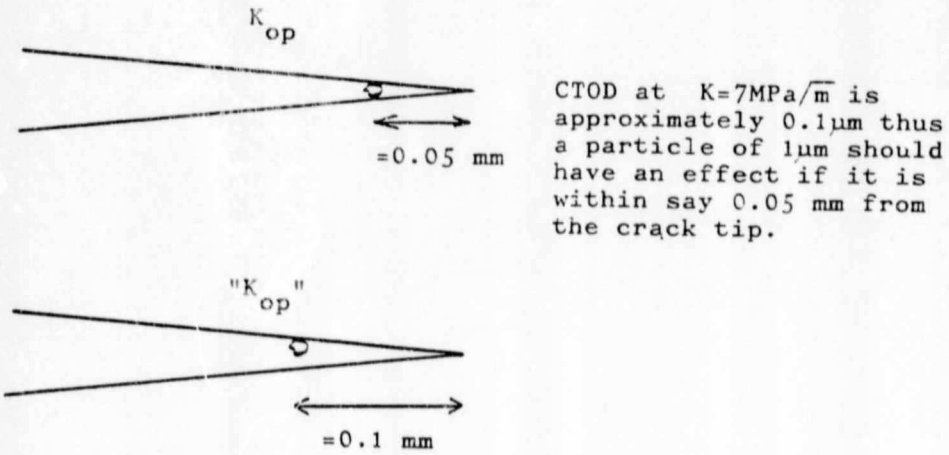

Figure 4.4 Illustration of wedgeing effect caused by a particle a) close to the crack tip, b) far from the crack tip.

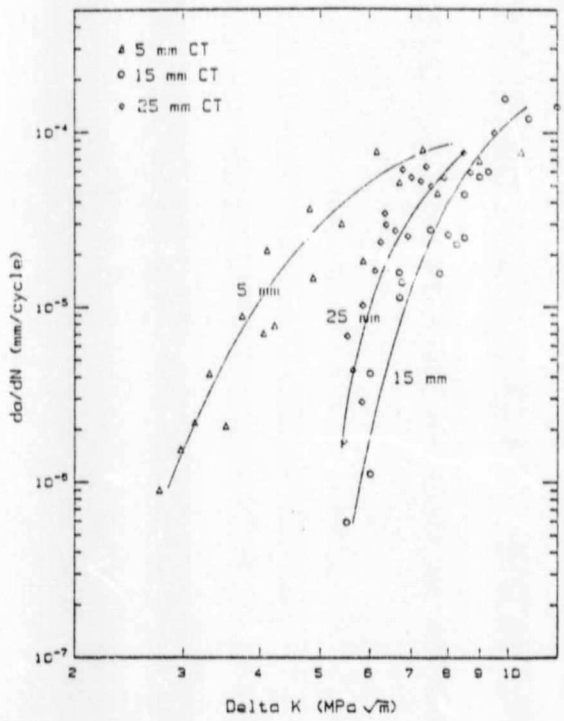

Figure 5.1 Growth rates in the AR condition for 5 mm, 15 mm and 25 mm thick CT specimens.

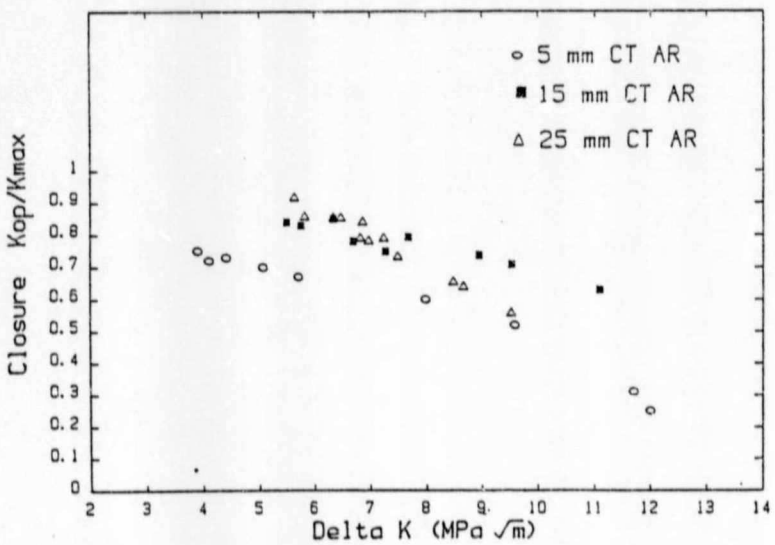

Figure 5.2 Closure data in the AR material for 5 mm, 15 mm and 25 mm thick CT specimens corresponding to growth rate data in Fig. 5.1.

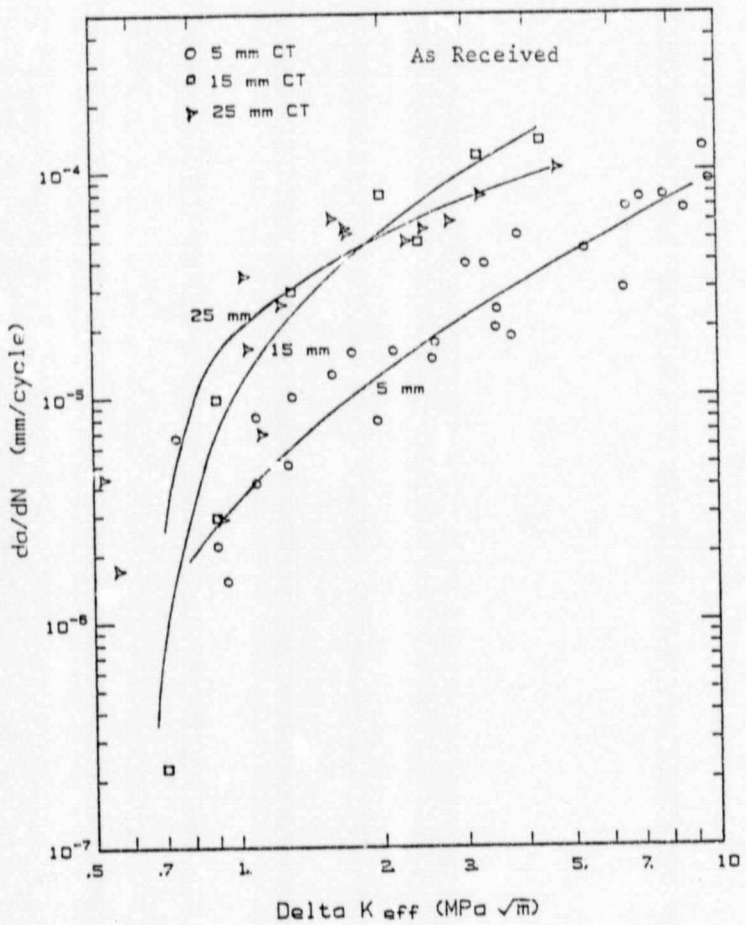

Figure 5.3 Growth rate vs ΔK_{eff}, illustrating the inability of closure concepts to reduce growth rates onto a single line.

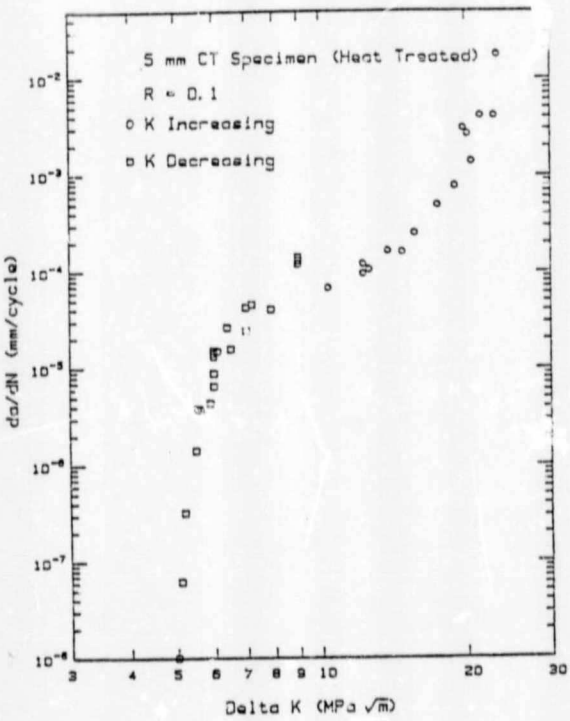

Figure 5.4 Growth rate data for 5 mm thick heat treated CT specimens at R = 0.1.

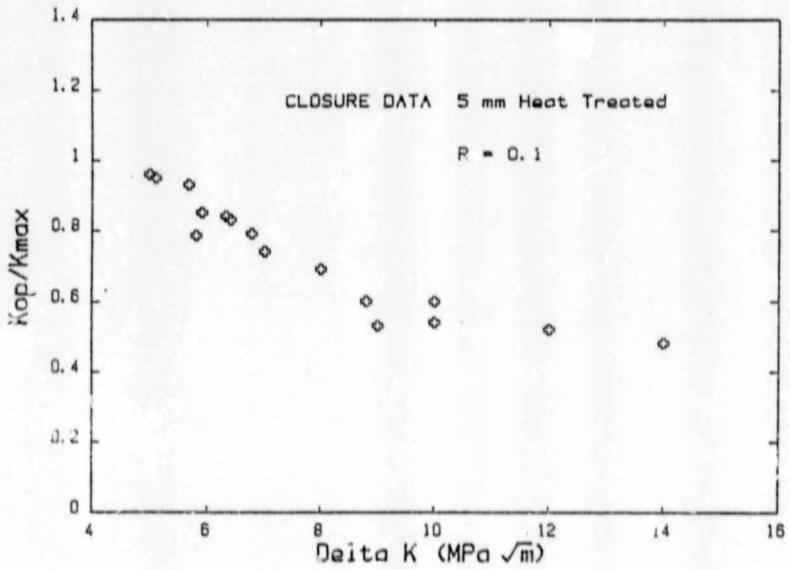

Figure 5.5a Closure data corresponding to growth rate data in Fig 5.4.

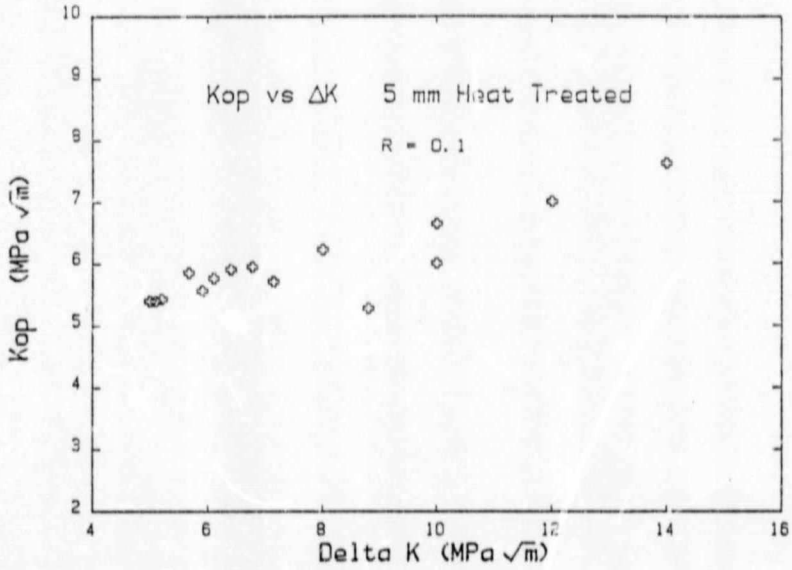

Figure 5.5b Closure data presented as K_{op} vs ΔK illustrating the consistency of the K_{op} magnitude.

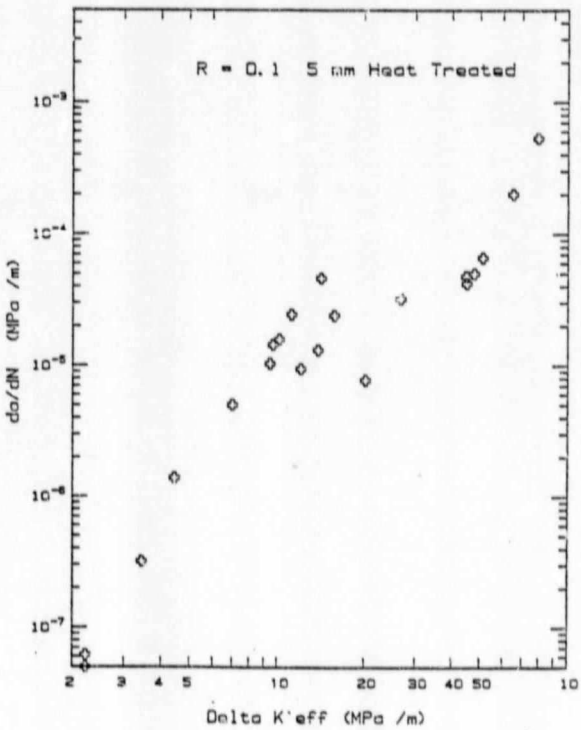

Figure 5.5c Growth rate presented as da/dN vs ΔK_{eff} for 5 mm heat treated CT specimens.

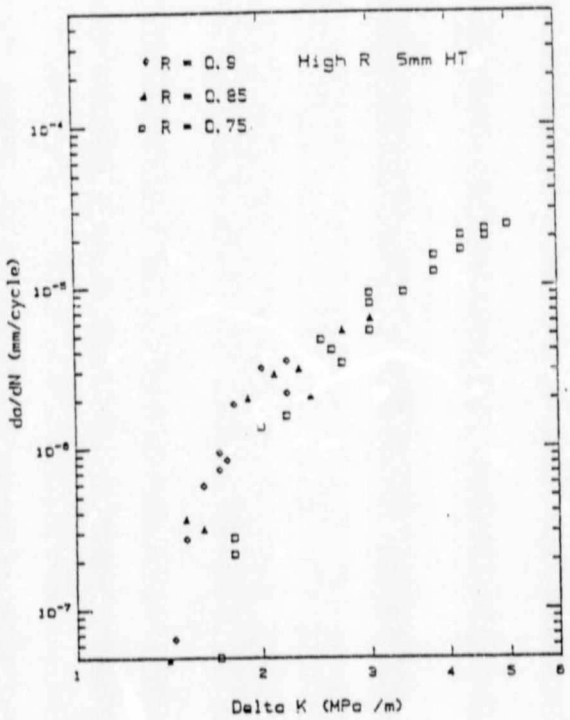

Figure 5.6 High R growth rate data for the heat treated material.

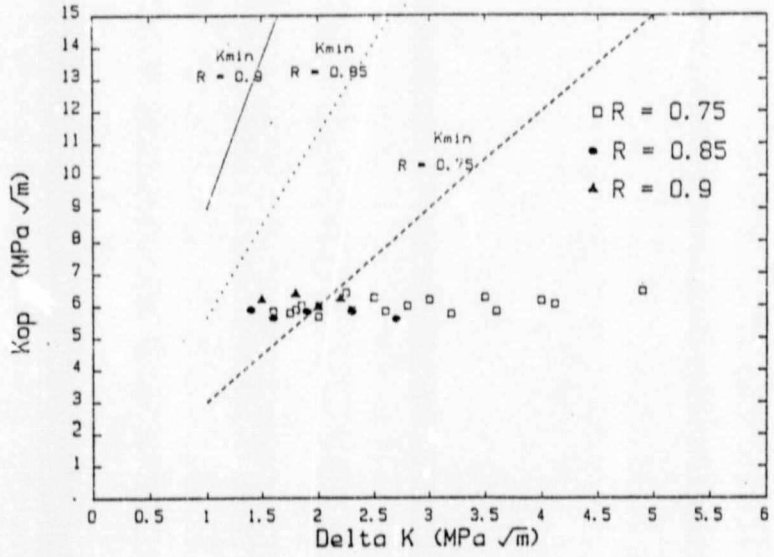

Figure 5.7 Closure presented as K_{op} vs ΔK for growth rate data presented in Fig 5.6.

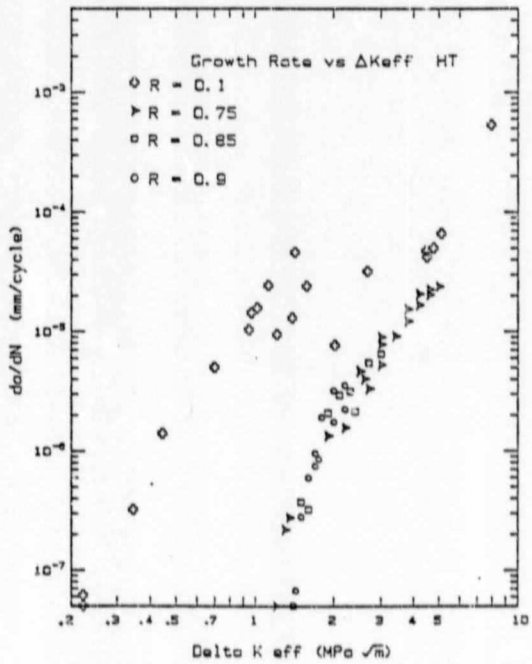

Figure 5.8 Growth rate vs ΔK_{eff} for 5 mm thick heat treated CT specimens.

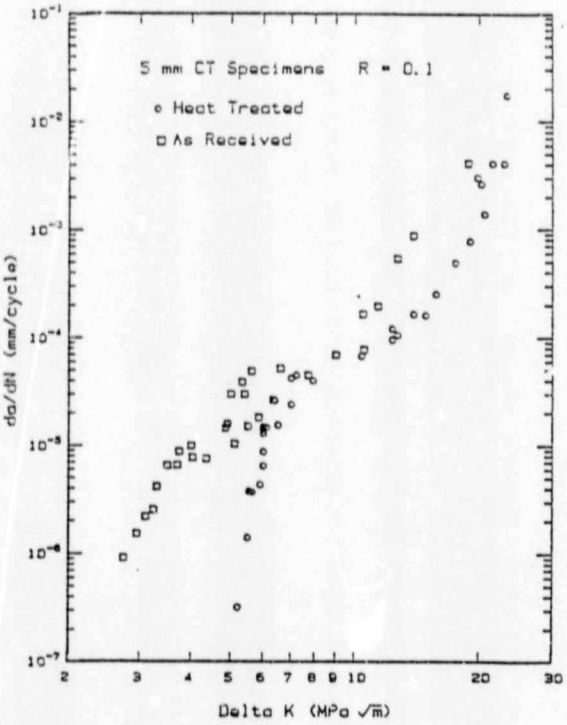

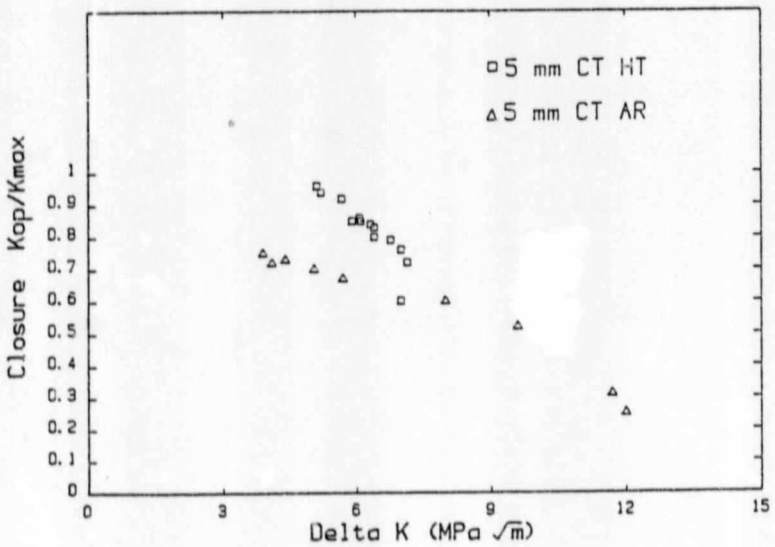

Figure 5.9 a) A comparison between the AR and HT growth rate data and the b) closure data .

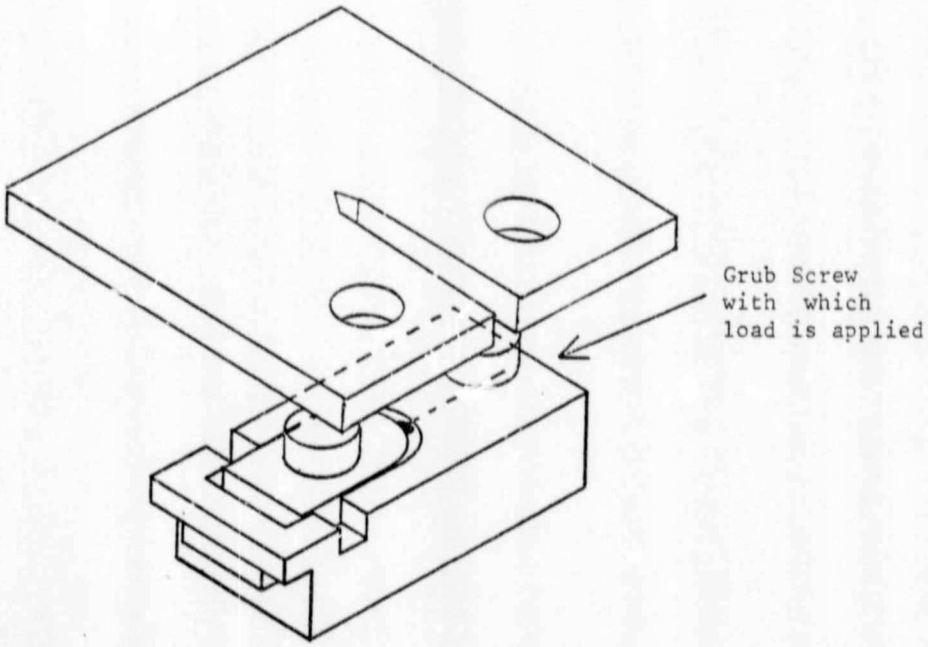

Figure 5.10 Straining gauge used to strain CT specimens in the SEM.

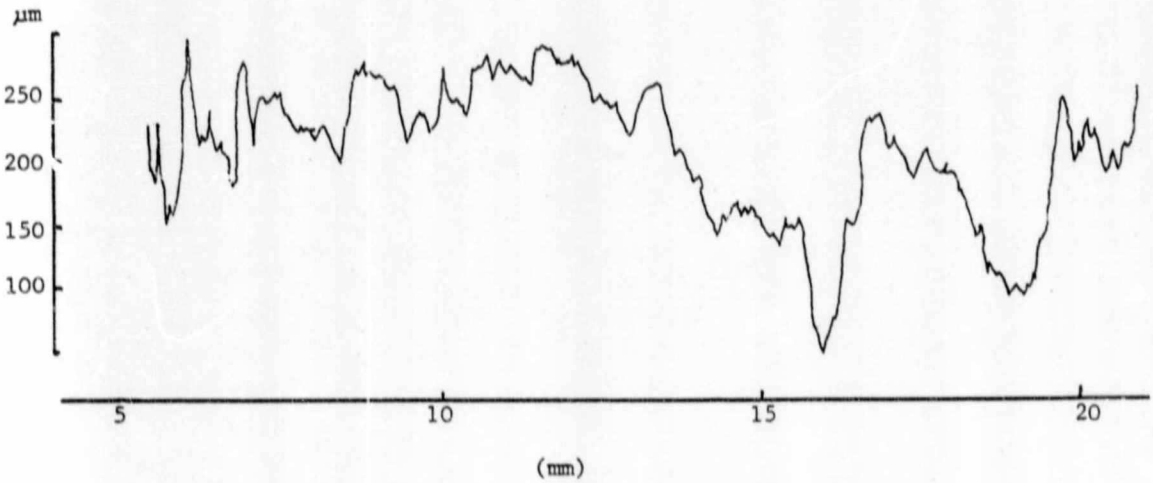

Figure 5.11 Roughness trace of the fracture surface for a 25 mm thick CT specimen in the AR condition.

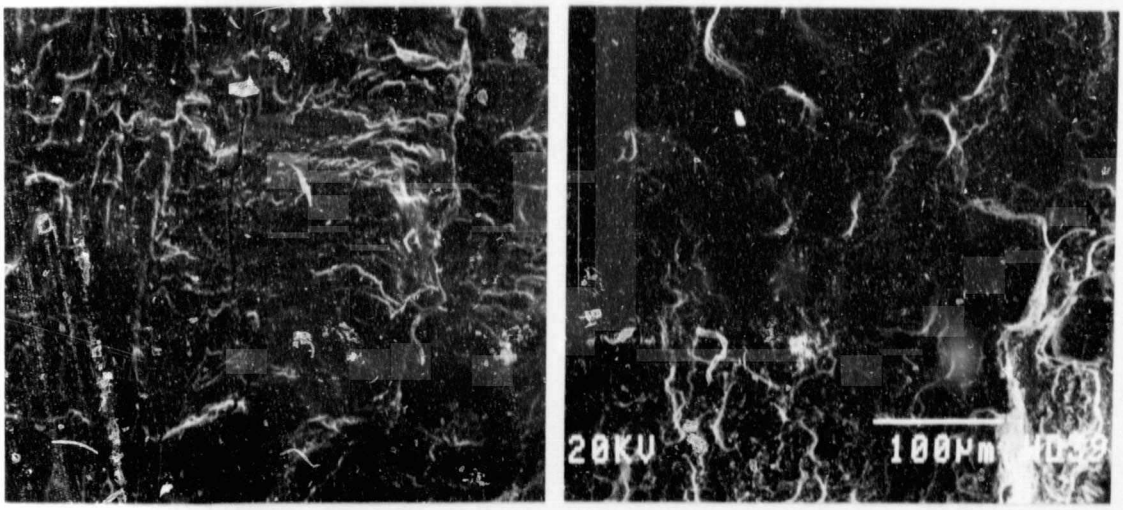

Figure 5.12 Fractographs of fracture surfaces representative of growth rates a) below 10^{-4} mm/cycle and b) above 10^{-4} mm/cycle.

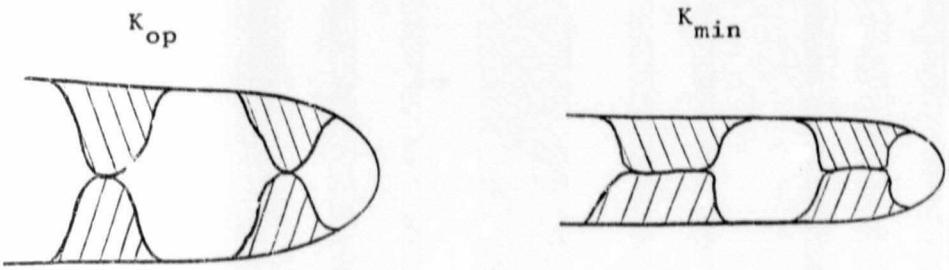

Figure 5.13 Schematic representation of the possible strain intensification due to limited asperity contact.

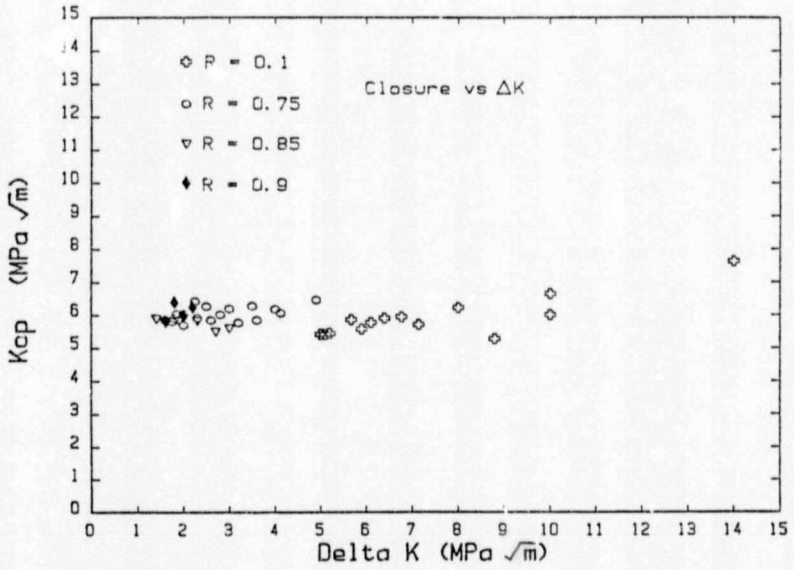

Figure 5.14 Closure data for all R ratios tested in the heat treated condition.

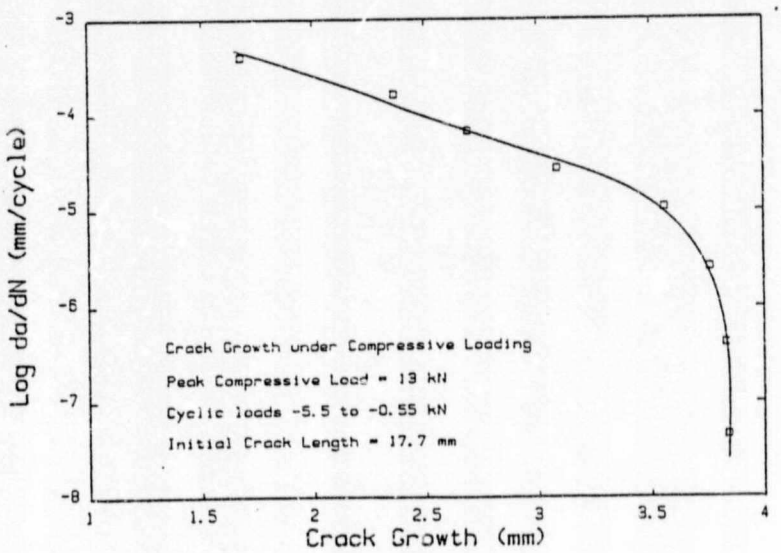

Figure 5.15 Fatigue crack growth under compressive loading.

a)

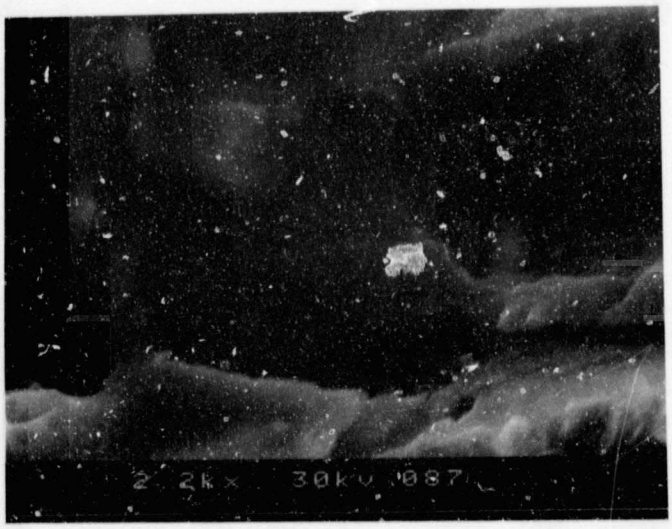

b)

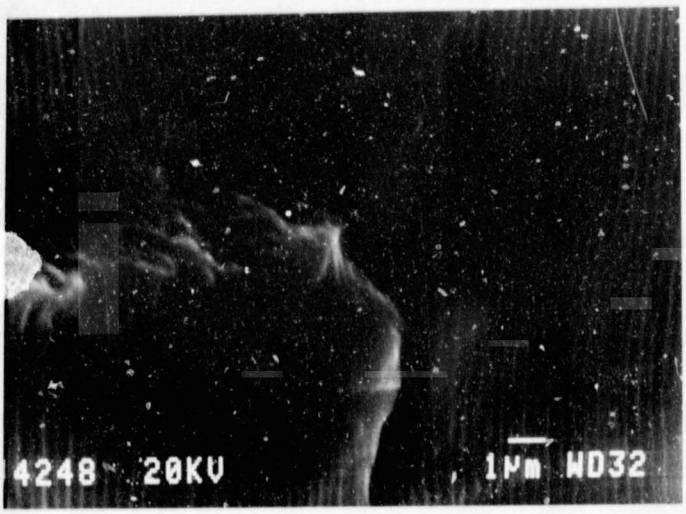

Figure 5.1 Fatigue striations produced by growth under a) tensile loading and b) compressive loading.

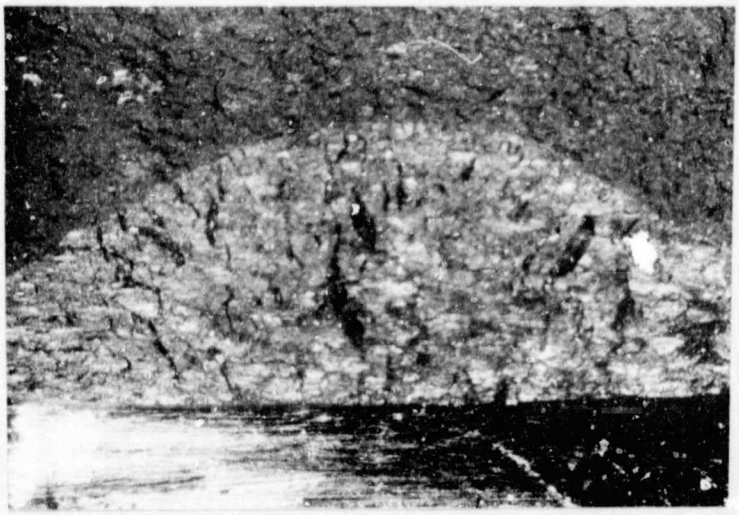

Figure 6.1 Fractured 25 mm thick CT specimens showing extensive curvature along the crack front.

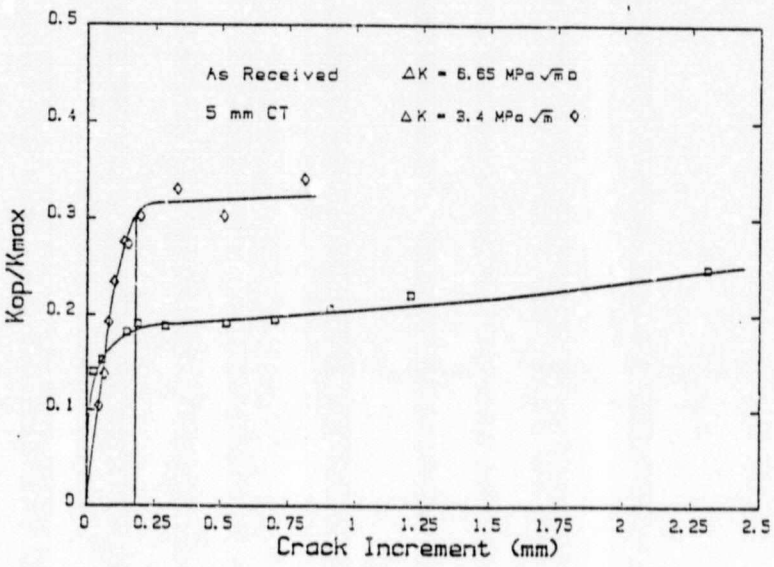

Figure 6.2 Closure development for the AR material after closure had been eliminated by wake removal and a compressive overload.

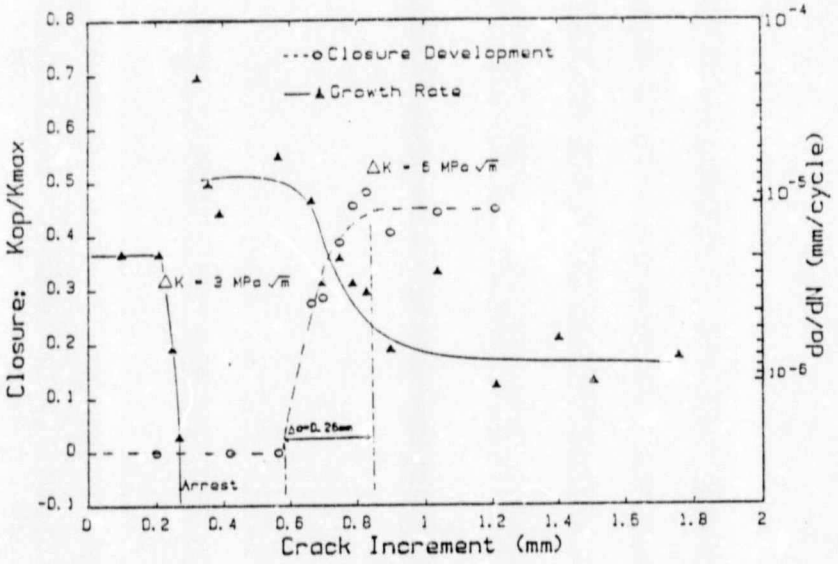

Figure 6.3 Closure development in the HT material at ΔK = 3 MPa$\sqrt{m}$ followed by closure development at ΔK = 6 MPa$\sqrt{m}$.

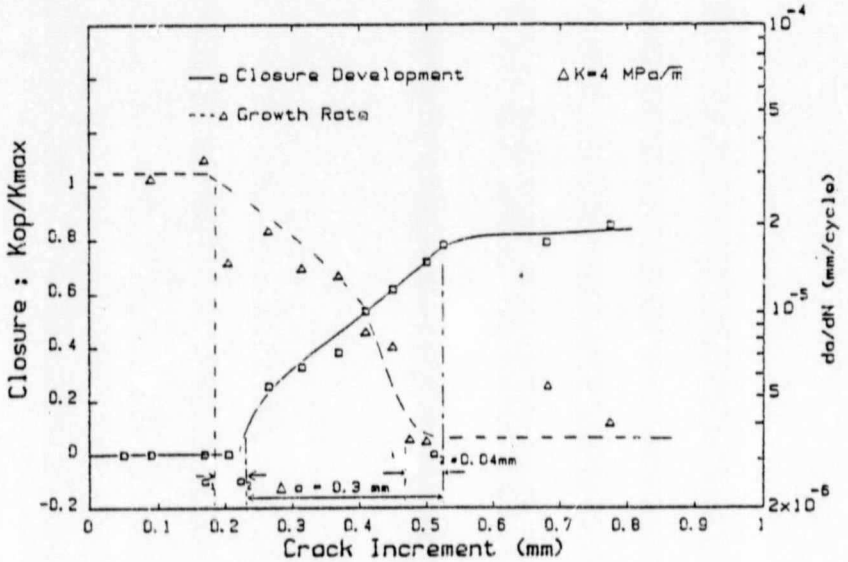

Figure 6.4 Closure development at ΔK = 4 MPa$\sqrt{m}$.

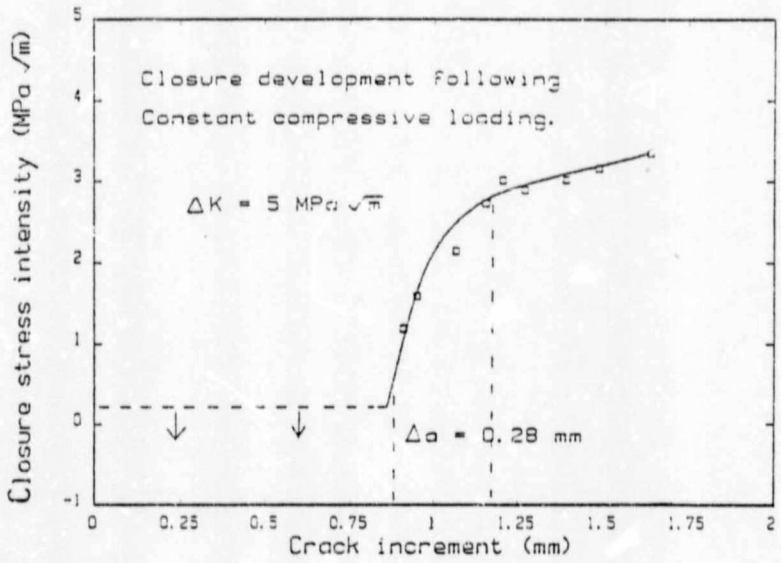

Figure 6.5 Closure development at ΔK = 5 MPa/m.

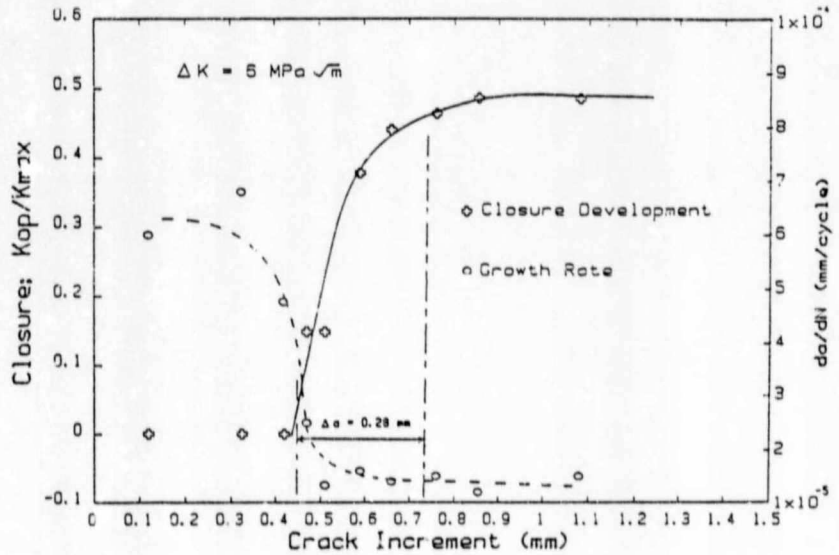

Figure 6.6 Closure development at ΔK = 6 MPa/m.

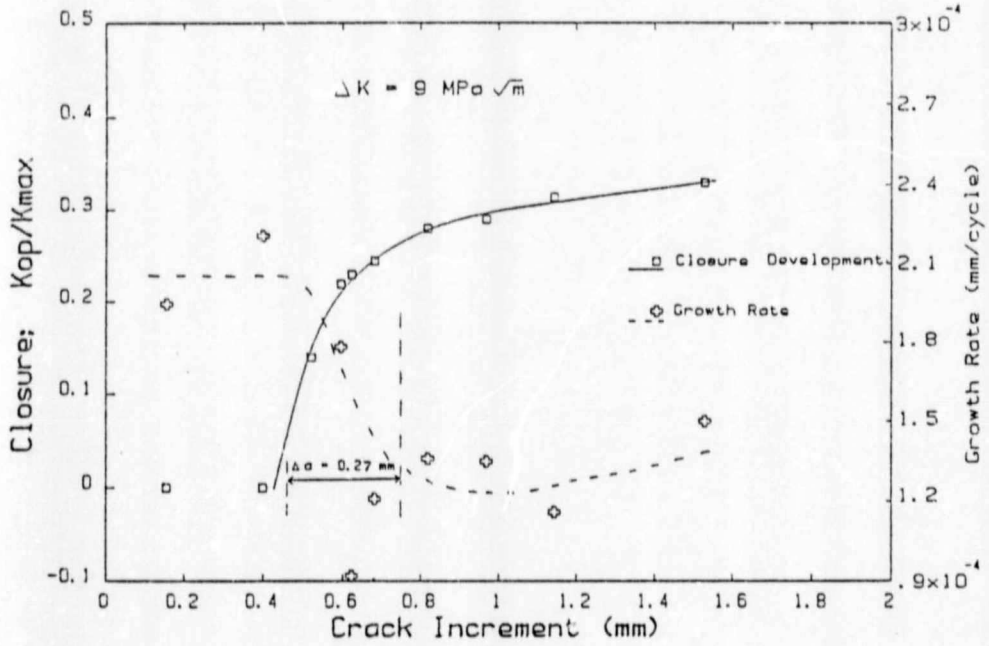

Figure 6.7 Closure development at ΔK = 9 MPa√m.

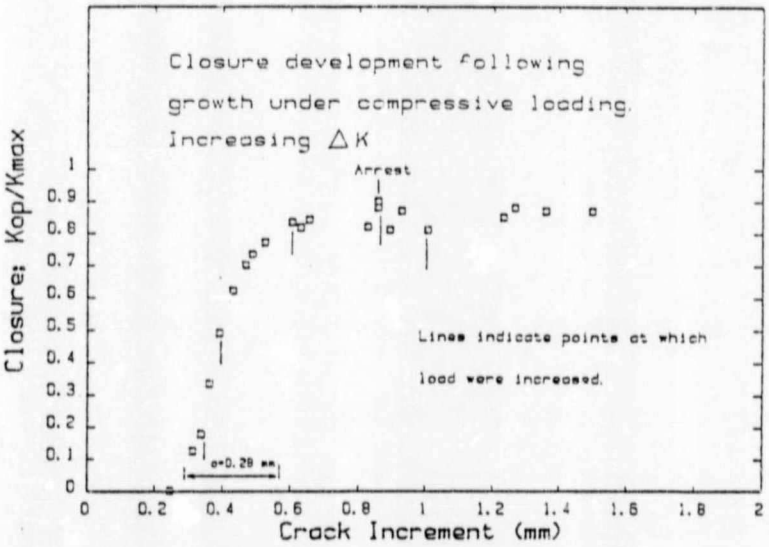

Figure 6.8a Closure development for increasing ΔK, starting with ΔK = 1.56 MPa√m.

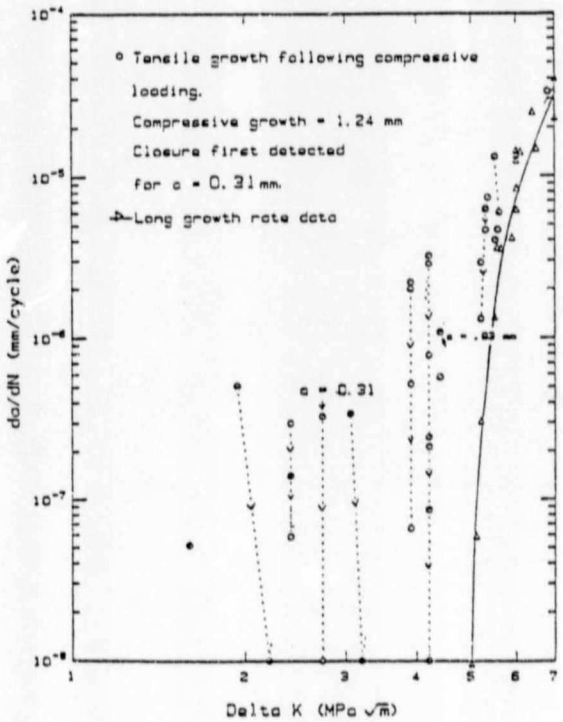

Figure 6.8b Fatigue crack growth rates obtained from an increasing ΔK method, after a crack had been produced under compressive cyclic loading.

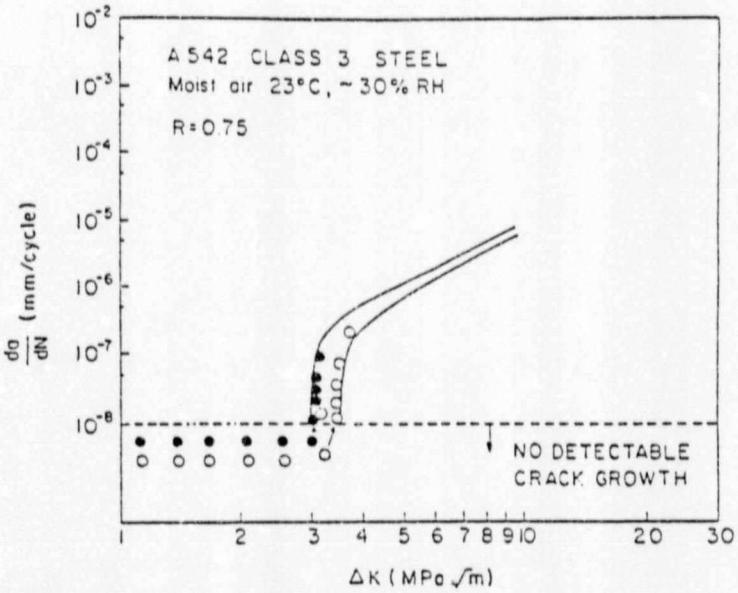

Figure 6.9 Fatigue crack growth at R = 0.75. Comparing growth rates obtained during load increasing schemes after a crack had been developed under compressive loading (circles) with growth rates obtained during load shedding (band indicated by the solid lines), (after Suresh et al [23]).

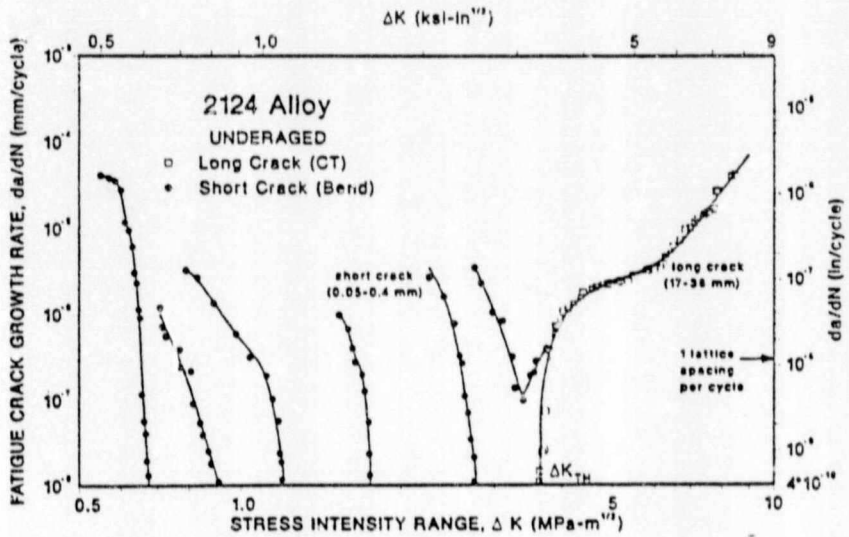

Figure 6.10 Fatigue crack growth rates in a 2124 T351 alloy at R = 0.1 for short and long crack growth. ΔK had to be increased continually to allow short crack growth to continue.

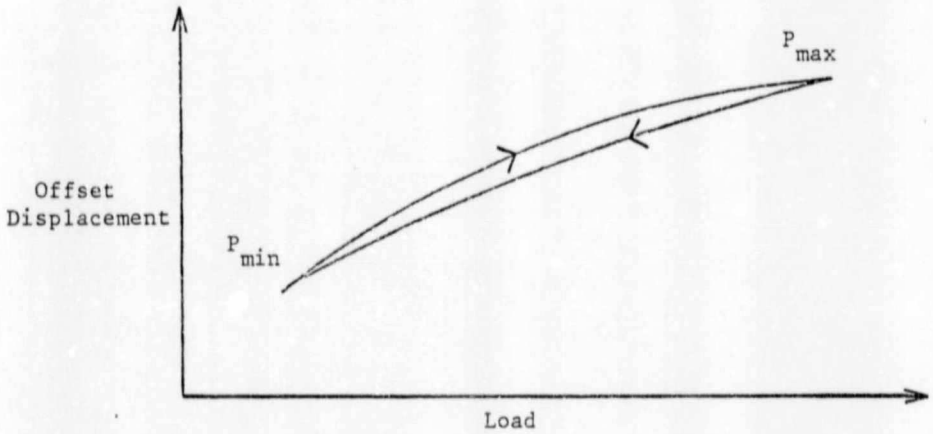

Figure 6.11 Offset displacement vs load traces obtained from BFS gauges showing uncharacteristic curvature.

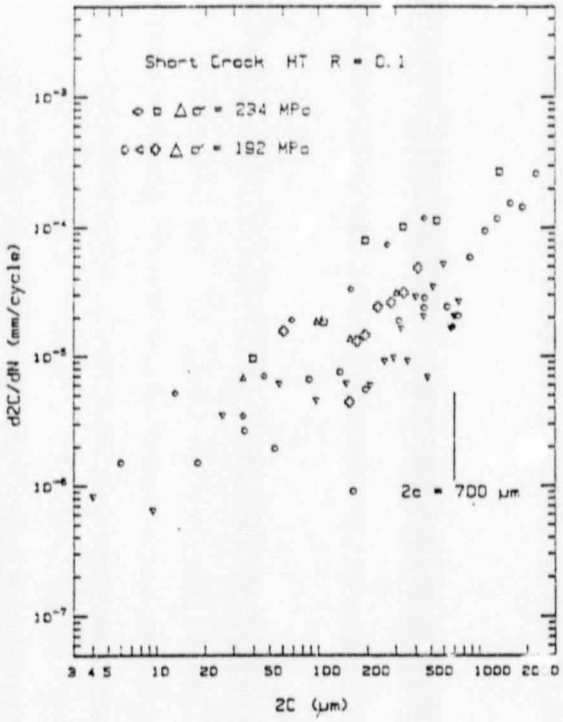

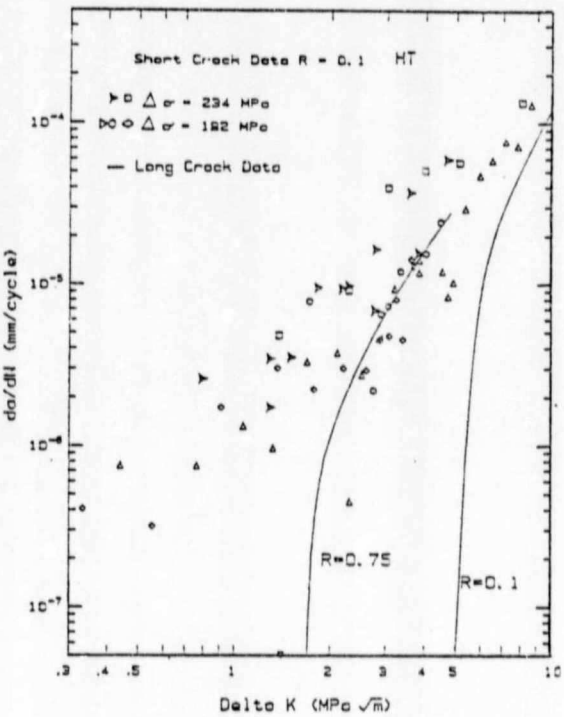

b)

Figure 7.1 Short crack growth data for the HT material at R = 0.1 plotted as a) da/dN vs 2c and b) da/dN vs ΔK.

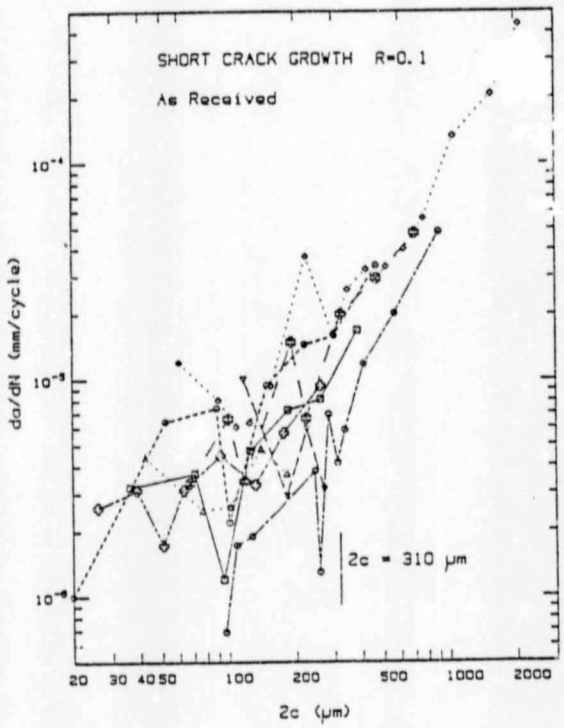

a)

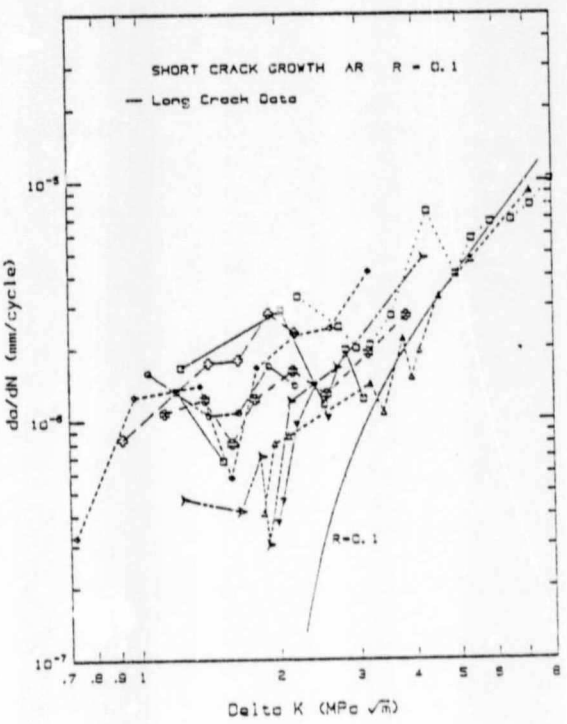

b)

Figure 7.2 Short crack growth data for the AR material at R = 0.1

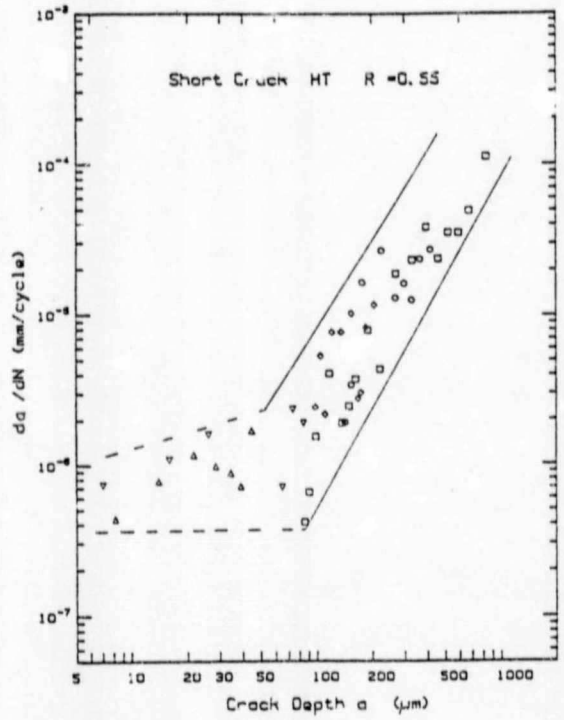

Figure 7.3a Short crack growth rates at R = 0.55 for the HT material.

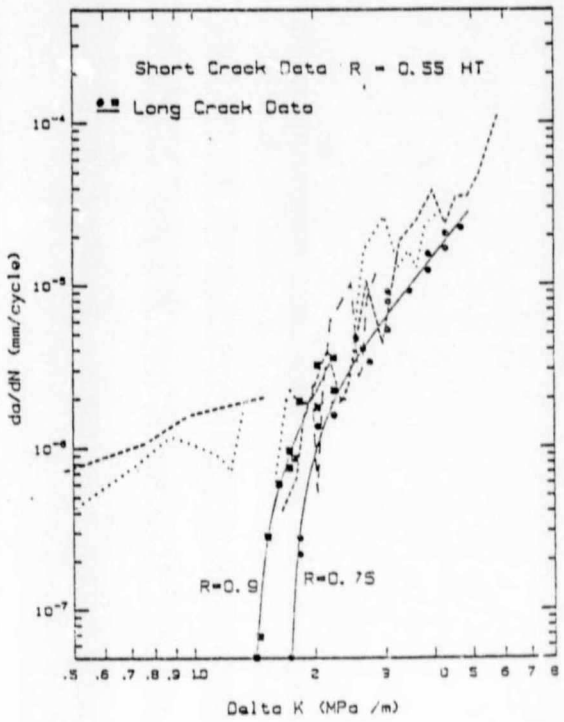

Figure 7.3 b) Comparison between short and long crack data in the HT material.

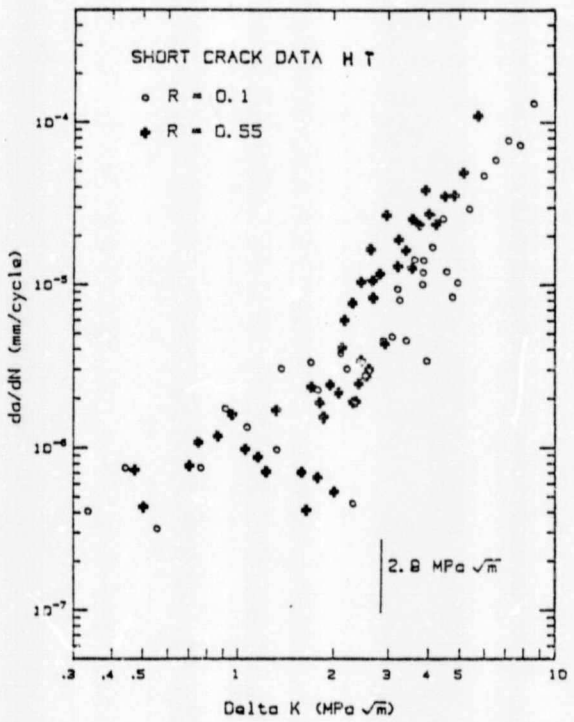

Figure 7.4 Comparison between short crack data at R = 0.1 and R = 0.55 for the HT material showing a difference in growth rates for ΔK ranges greater than 2.2 MPa$\sqrt{m}$.

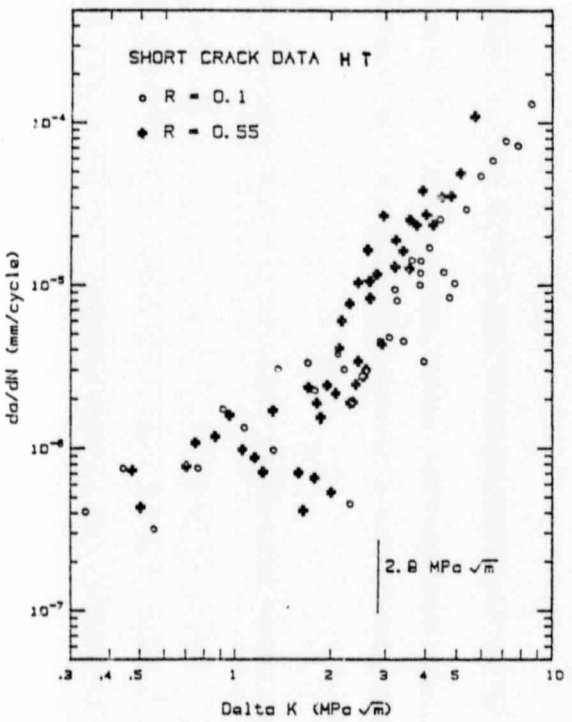

Figure 7.4 Comparison between short crack data at R = 0.1 and R = 0.55 for the HT material showing a difference in growth rates for ΔK ranges greater than 2.2 MPa$\sqrt{m}$.

Author Garz Reiner Ernst
Name of thesis Fatigue Crack Closure And Closure Development In A High Strength Aluminium Alloy. 1988

PUBLISHER:

University of the Witwatersrand, Johannesburg
©2013

LEGAL NOTICES:

Copyright Notice: All materials on the University of the Witwatersrand, Johannesburg Library website are protected by South African copyright law and may not be distributed, transmitted, displayed, or otherwise published in any format, without the prior written permission of the copyright owner.

Disclaimer and Terms of Use: Provided that you maintain all copyright and other notices contained therein, you may download material (one machine readable copy and one print copy per page) for your personal and/or educational non-commercial use only.

The University of the Witwatersrand, Johannesburg, is not responsible for any errors or omissions and excludes any and all liability for any errors in or omissions from the information on the Library website.